A STUDY OF SHOCK WAVE TURBULENT BOUNDARY LAYER INTERACTION AT M = 3

S.M. Bogdonoff, C.E. Kepler, and E. Sanlorenzo

Report No. 222, July 1953

UNITED STATES NAVY

Office of Naval Research
Mechanics Branch

and

UNITED STATES AIR FORCE

Office of Scientific Research

Contract No. N6-onr-270, Task Order No. 6, Project Number NR-061-049

ACKNOWLEDGEMENT

The present study is part of a program of theoretical and experimental research on viscous effects in supersonic flow being conducted by the Gas Dynamics Laboratory, Forrestal Research Center, Princeton Universtiy. This research is sponsored jointly by the Office of Naval Research (U.S.N.), Mechanics Branch and by the Office of Scientific Research (U.S.A.F.) under Contract Number N6-onr-270, Task Order No. 6, Project Number NR-061-049.

TABLE OF CONTENTS

	Page
SUMMARY	
INTRODUCTION	1
EXPERIMENTAL EQUIPMENT AND TECHNIQUES	2
NOMENCLATURE	6
CHECKS ON THE VALIDITY OF THE DATA	6
RESULTS AND DISCUSSION	
Wall Static Pressure Distribution and Optical Studies	9
Separation and Reattachment	13
Interaction Models	14
Corrected Boundary Layer Profiles	17
GENERAL DISCUSSION	18
CONCLUSIONS	19
REFERENCES	21
APPENDIX A	22
APPENDIX B	26

SUMMARY

An experimental study has been made of the effect of the interaction of varying strength shock waves with a turbulent boundary layer at a Mach number of about 2.9. It was not possible to obtain two-dimensional interactions with shock generators which did not completely span the tunnel or for shock strengths less than a pressure ratio of about 1.5. Below an incident shock pressure ratio of 1.7, the interaction is similar to the theoretical inviscid case. The incident shock is reflected as a single compression, no separation exists and the pressure rise on the wall is smooth and occurs in about two to three boundary layer thicknesses. Above an incident shock pressure ratio of 1.7, separation is evidenced by a "bump" in the wall static pressure curves and bifurcation of the incident shock wave. The reflected system now consists of a compression-expansion-compression region. There is some indication that the incident shock pressure ratio for separation appears to be independent of Mach number. Separation occurs about two boundary layer thicknesses from the beginning of the interaction at a wall static pressure ratio of about 2. This phenomena is independent of shock pressure ratio over the range tested. For high strength shocks, pressure ratios of the order of 3, increases in shock strength change the scale of interaction region without changing its structure. In this region the various parts of the interaction are sufficiently separated for individual detailed studies. There are considerable discrepancies between the data presented herein and those presented by Gadd, Holder, and Regan. This may be due in part to the wedge spans used by these investigators.

A STUDY OF SHOCK WAVE TURBULENT BOUNDARY LAYER INTERACTION AT M = 3

INTRODUCTION

During the past few years, the interaction of a shock wave with a boundary layer has been the subject of considerable theoretical and experimental investigation. The large deviations from the theoretical inviscid reflection of a shock wave from a solid wall are of considerable practical importance in supersonic diffusers, deflected control surfaces on supersonic wings, and other applications. The work of Leipmann[1] and others[2] has provided a considerable body of experimental data on the interaction of a shock wave with laminar layers. Several authors[3,4,5,6] have made considerable progress with theoretical studies of both laminar and turbulent interactions. All of these theories, however, depend on obtaining certain factors from the experimental results. Several studies of the interaction of shock waves with turbulent boundary layer have also been made. [7,8,9,10] However, the data available is still insufficient to provide a detailed model of the interaction phenomena.

As part of a broad program of research on viscous effects in supersonics being conducted by the Gas Dynamics Laboratory, Aeronautical Engineering Department of Princeton University, an attempt is being made to obtain data on shock wave boundary layer interactions over a very wide range of Mach numbers, Reynolds numbers, and shock strengths. Such a detailed experimental analysis is required as a preliminary to a complete

theoretical solution of this complicated problem. The results presented herein are a part of this over-all program and have been restricted to results at a Mach number of 3 for one turbulent boundary layer with varying shock strengths. The study has consisted of examining the interaction problem by 1) measuring the static pressure distribution on the wall, 2) making total head surveys through the interactions, and 3) using optical techniques to obtain photographs of the flow. These techniques include conventional shadowgraph and Schlieren techniques and the use of some special color Schlieren techniques described more fully later in the report. The main purpose of this series of tests was to examine, in detail, the structure of the interaction region and how it is affected by varying shock strengths. Some errors in Reference 9 are also corrected herein. This work was carried out under the joint sponsorship of the Office of Naval Research, Mechanics Branch, and the Office of Scientific Research, Air Research and Development Command, U.S. Air Force, Contract Number N6-onr-270.

EXPERIMENTAL EQUIPMENT AND TECHNIQUES

The experiments were performed in the Princeton University Pilot supersonic tunnel[11] at a Mach number of approximately 2.92. The wind tunnel is the "blow-down" variety utilizing air stored at 3000 psi in tanks of a total capacity of 170 cubic feet. A regulator between the tanks and the tunnel permits operation at any desired stagnation pressure between 75 psi and 900 psi; but for the tests herein reported it was operated at a pressure level of about 100 psi. Running times were of the order of five minutes with a test section 2" wide and 2½" high.

A wedge, spanning the tunnel, was used for a shock generating device, and the boundary layer on the flat section of the tunnel wall was utilized for the measurements. The static pressure on the wall was measured by a .030" orifice on the tunnel centerline. At this station the undisturbed boundary layer thickness was approximately .17 inches. The wall static pressure data presented was taken using the single orifice as the interaction was passed over it. Thus, errors in using numerous static pressure holes were eliminated, and the data points could be spaced as closely as desired. In some cases, additional wall static pressure orifices 3/4" to the front and rear of the main (aforementioned) one were used to check the interaction at different stations in the tunnel. Additional spanwise static pressure orifices were used to check the two-dimensionality of the interaction. These were located 3/8"; 1/2"; 5/8"; and 3/4" off axis, but at the same station as the main orifice.

Several shock generators (wedges) were used, each held in the free stream by a supporting frame driven by a micrometer. (See Figures 1 and 2). The micrometer drive permitted closely controlled movement of the wedge in the tunnel. Three variable angle wedges were used covering nominal deflection angles of 0° to 7°, 6° to 12°, and 9° to 15°. Each of these spanned the tunnel to within .010" of the side walls. To check the effect of end gap, two 10° (fixed nominal angle) shock producing wedges were employed which differed in width, the narrower one being 1 1/4" wide and the other nearly 2" wide (a full span wedge). Wedges were provided with a static pressure orifice drilled on centerline 1/2" from the leading edge. In addition, the medium angle wedge (6° to 12°) and the full span

10° fixed angle wedge had a similar orifice located 1" from the leading edge. The pressure ratio of the generated shock was determined by using this static pressure rather than the geometrical wedge angle, thus taking into account any effect of the boundary layer on the wedge, inaccuracies in setting, and irregularities in the tunnel flows.

Total pressure surveys were made parallel and normal to the tunnel wall employing a total head tube constructed of .065" O.D. steel tubing flattened at the end and honed on the bottom surface to allow a close approach to the wall. The orifice was .004" high by .060" wide and the bottom surface was .002" thick. Thus, readings to within .004" of the surface were obtainable. The total head probe was set in an insulated mount so an electrical contact could determine when the total head tube was just touching the surface. The micrometer drive on which the probe was mounted permitted displacements perpendicular to the wall accurate to within .001". For every survey the "just touching" position was established with the tunnel running since pre-setting of the probe might be erroneous due to deflection of the probe during the run or the start.

All static pressures were measured with differential pressure gages; calibrated and accurate to within .5 inches of water. In some instances two such gages were connected in series to enable readings over wider pressure ranges. Since the static pressures encountered were the order of 100 inches of water, the accuracy is within 1%. All total pressure measurements were made with absolute pressure gages, calibrated and accurate to within .2 inches of mercury, with a resulting accuracy of 1%

for the pressures measured. Stagnation pressure was measure with a high precision bourdon gage also accurate to within 1%.

Difficulty was encountered starting the tunnel with the wedge set at high angles. This was circumvented by: 1) starting with the wedge set at a relatively low angle and adjusting to the desired flow deflection angle with the tunnel running and, 2) cut-outs in the downstream end of the nozzle blocks to relieve blockage caused by the wedge angle changing mechanism. The step (cut-out) on the bottom wall was several inches downstream from the wall static pressure orifice. It was used also to check the effect of a downstream disturbance (expansion) on the interaction. (See section Checks on Validity of Data.)

Optical techniques, supplementing the pressure measurements, were used to study the phenomena. The conventional skewed bi-parabolic mirror Schlieren system was used and adapted for shadowgraph pictures as well. Thus, Schlieren pictures, both horizontal and vertical cut off, as well as shodowgraph pictures, were taken for each condition. The light source was a high pressure spark resulting in exposures of the order of a microsecond. In addition, Schlieren photographs were also taken in color. Basically, the system consisted of inserting a prism in the light path after the source which effectively changes the point source to a spectral line. The knife edge at the second focal point is then replaced by a slit which can be adjusted to permit any of the spectral colors for the base (no flow) condition. In such a system, regions with the same density gradient will exhibit the same color, contrasting to the conventional black and white system in which such regions would be of the

same gray scale. Colored Schlieren photographs are not new, but the techniques used here (described in detail in Appendix A and B) permitted excellent resolution with a microsecond exposure. The combination of color and the short exposure time permitted an analysis of the structure of the interaction region not heretofor possible by optical means.

NOMENCLATURE

x	distance along tunnel wall, inches
y	distance normal to tunnel wall, inches
P	static pressure measured on tunnel wall
P_o	chamber pressure
P_1	static pressure ahead of interaction
P_2	static pressure behind generated shock (as measured on shock generator)
P_3	static pressure after interaction
M	Mach number
θ	nominal wedge angle (flow deflection angle, degrees)
δ	boundary layer thickness, inches

CHECKS ON THE VALIDITY OF THE DATA

A study of the results available on shock wave boundary layer interactions showed that many investigations had been made using shock generators which did not fully span the tunnel. This was usually done to obtain Schlieren and shadow photographs which were sharper than those obtained with a wider wedge whose shock wave interacted with the side wall boundary layers. No data was available, however, to determine the effects of these side wall gaps which, in most cases, were of the order of a boundary layer thickness. Preliminary studies[9] of the shock wave

boundary layer interaction were first carried out using nominal 10° wedges, of 1½" and full 2" span. Figure 3 presents the wall static pressure variation on centerline using the "narrow" wedge in juxtaposition with a sketch of the interaction. It can be seen here that the pressure peaks and then falls to a value after the interaction which is much less than the theoretical value. The overall pressure rise as measured is about 2.5, whereas, the theoretical rise (based on the static pressure as measured by the orifice on the wedge) should be about 3.8. The spanwise static pressure orifices in the tunnel were used to check the two-dimensionality of the flow. The results shown in Figure 4 exhibit a considerable deviation from two-dimensional flow and indicate a relieving effect due to the presence of spanwise flows. The tests were repeated, using the full span wedge (i.e., clearance to within .01") and resulted in the static pressure distribution shown in Figure 5. The final pressure is quite close to the theoretical value and the pressure distribution is of a considerably different shape than that obtained for the narrow wedge. The spanwise pressure surveys, Figure 6, show that two-dimensional flow has been achieved. All subsequent tests herein reported were, therefore, made with full span wedges and the results were checked for two-dimensionality.

Studies of weak shock interactions (flow deflection from 0° to 6°) resulted in wall static pressure distributions along centerline which exhibited a definite peak. There was no constant pressure region after the interaction, similar to the distribution shown in Figure 3 for a 10° shock using a narrow wedge. Checks for two-dimensionality, using the

spanwise orifices, indicated cross-flows piling up on one side of the tunnel or the other. This pattern differs from the non-two-dimensional flow found using the narrow wedge in which the spanwise distribution of pressures tended to be symmetrical about the centerline. Further attempts to make the flow two-dimensional, such as completely sealing the small end gaps of the shock generator, did not yield satisfactory results. It appears as if the effects of tunnel disturbance such as interaction of the boundary layer on the walls and floors of the tunnel, and interaction of the shock with the side wall layers, are of the same order of magnitude as the disturbance caused by the studied interaction. This would, in the whole, probably depend on the exact experiment set-up and would vary from tunnel to tunnel. These phenomena in the shock wave boundary layer interaction have not been noted by previous investigators due to the absence of a stringent test for two-dimensionality and the results obtained are open to some question in light of the possible existence of such cross flows. The above results restricted the study reported herein to shock strengths above 6° where two-dimensional flows could be obtained.

Examination of a typical strong interaction (for example, Figure 5) introduced another doubt as to the validity of the data. The pressure rise now spreads over a considerable distance, and the proximity of the interaction region to the expansion fan from the rear corner of the wedge prompted an investigation to determine the effect of such a downstream disturbance. A step cut in the tunnel wall was utilized for this study. Schlieren photographs were taken as the interaction was moved downstream over the step. In all cases, the step disturbance had to be

located at least two boundary layer thicknesses ahead of the impingement point of the expansion fan before an effect was felt. All high angle data was checked by the aforementioned method and although, for angles 11° through 15°, the expansion fan intersected the boundary layer before the full pressure rise was realized, the position of its impingement was always after the station where the step first produced a noticeable change. Since the flow over such a step results in a pressure gradient far stronger than that encountered in the expansion from the wedge, its effect should be greater, and hence it is felt that the expansion fan has little effect upstream of its intersection point.

The steadiness of the flow was checked by taking high speed Schlieren motion pictures with a "Fastax" camera operating at 8000 frames per second. An examination of these photographs showed very slight oscillations of the first reflected shock which appeared to be of the order of less than 1/10 of the boundary layer thickness, i.e., less than 0.02 inches. The rest of the phenomena appears completely steady. Since the pressure measurements essentially represent "long time averages" these slight oscillations of the first reflected shock wave do not appear in the results. This examination was carried out only for a nominal shock strength of 13°.

RESULTS AND DISCUSSION

Wall Static Pressure Distribution and Optical Studies

The wall static pressure distributions through the interactions of varying strength shock waves with a turbulent boundary layer are shown in Figures 7 through 15. In Figure 16, the curves for all the interactions are superimposed using the same zero point. This zero point was picked

from Schlieren and shadow photographs as the point of impingement of the experimental incident shock with the wall if no boundary layer were present. For the high angles, (θ = 11° through 15°) the vertical line at the top of the pressure curve indicates the position at which the expansion fan from the rear of the wedge strikes the boundary layer. In Figure 18, the corresponding Schlieren and shadow photographs are presented. A comparable color Schlieren photograph is shown in Figure 19.

For ease of identification, tests are designated by the nominal shock deflection angle, θ. A more truly representative quantity is the pressure ratio across the incident shock which was measured directly by the static pressure orifice on the wedge. The actual shock pressure ratios are tabulated below.

θ	P_2/P_1
7°	1.60
8°	1.70
9°	1.78
10°	1.90
11°	2.27
12°	2.37
13°	2.51
14°	2.90
15°	3.10

For shock strengths through 10°, the pressure ratios noted are constant within 2% for the entire interaction. For stronger strength shocks, increased movement of the wedge was necessary to survey the spread out interaction region. Due to axial variation of Mach number in the tunnel, the accuracy of the pressure ratio decreased and for the highest angle (15°), was only 10%. Fortunately, for strong shocks, these variations had little effect on the wall pressure distributions.

An examination of the pressure curves reveals that, for weak shocks ($\theta \sim 7°$), the static pressure rise is smooth and rapid and the entire phenomena occurs within two to three boundary layer thicknesses. A study of the photographs shows that the incident shock penetrates deep into the boundary layer from whence the reflected compression wave originates. As expected, the boundary layer is thinner after the interaction than before. The phenomena, with the exception of the bending of the shocks in the boundary layer, is quite analogous to the theoretical reflection of a shock from a solid wall.

As the shock strength is increased to $\theta \sim 9°$, the interaction is spread to four or five boundary layer thicknesses. From the pressure curves one can first experimentally verify the presence of a "bump" or inflection point at $\theta \sim 8\frac{1}{2}°$, (incident shock pressure ratio of ~ 1.75). The initial slope is still very steep, the inflection region accounts for the increased length of the interaction. From the photographs, at these angles, one first sees the "bifurcated foot" of the interaction. The reflected wave and the incident wave cross within the boundary layer, exhibiting [illegible]ropagation forward of the interaction. The incident wave

reflects as from a free jet (constant pressure boundary) causing an expansion region which turns the flow back towards the wall. This is followed by a region of slow compression. There is a dark region at the foot of the interaction indicating separation. Color Schlieren photographs show clearly the change of the phenomena from a single reflected compression for the weak shock interaction to the compression-expansion-compression region for the stronger interaction. Such photographs also show the very weak normal density gradients in the small region below the interaction. The boundary layer is still thinner after the interaction. For these shock strengths, the phenomena has changed considerably from the theoretical non-viscous model.

Further increase in shock strength to $\theta \sim 11^{\circ}$, spreads the interaction still further to seven or eight boundary layer thicknesses. The bump in the pressure curve is more pronounced and the intersection of the incident and reflected shocks occurs at the edge of the boundary layer. The expansion fan after the first reflected shock and the region of slow compression are spread a considerable distance downstream. The dark region below the interaction is quite pronounced and color Schlieren photographs indicate a zero vertical gradient in this region, i.e., separated flow, which will be shown conclusively later. Through this interaction the losses have increased such that the boundary layer thickness downstream is about equal to that before the interaction in spite of the highly increased pressure level. For strong shocks ($\theta \sim 13^{\circ}$), the interaction is spread to twelve or more boundary layer thicknesses; the "bump", now quite pronounced, comprises half of the interaction. The

reflected compression now extends a considerable distance out of the boundary layer before it intersects with the incident shock and the height of the interaction is two or more boundary layer thicknesses. There is a large separated region at the foot of the interaction.

Separation and Reattachment

To determine the point of separation and the extent of the separated region, total head surveys were made less than 1/10 of a boundary layer thickness from the wall (y = .014"). Using the wall static pressure distribution and the conventional pitot-static relationship, the Mach number distribution along the wall was obtained. For $\theta \sim 9^{\circ}$, separation was not detected. Although, the "bump" in the pressure curve for $\theta \sim 9^{\circ}$ indicated separation, the region is probably too small to pick up by this crude method. The distributions for shock strengths of 10°, 12° and 14° (Figures 20, 21, and 22) show a definite separated region. The pressure ratio for separation (static pressure at separation/ static pressure before interaction) in all three cases is about 2.0. This point corresponds, on the pressure curve, to the beginning of the "bump" in which the steep initial slope gives way to a much reduced slope in the separated region. As the shock strength is increased, the separated region grows rapidly; for the 10° case its length is of the order of a boundary layer thickness, for a 12° shock the order of three boundary layer thicknesses, for the 14° shock its extent is roughly seven boundary layer thicknesses.

The aforementioned results checking the effect of a downstream disturbance led to the finding of a "throat" in the interaction after

which no expansive disturbance had an effect on the upstream region of the interaction. This "throat" closely follows the point of reattachment of the separated flow. For the 10° and 12° case, the "throat" is of the order of one boundary layer thickness behind the reattachment point, and for the 14° case even closer. The closeness of the "throat" and the reattachment point indicates very high mixing rates in this region. The proximity of the "throat" and the separated region also explains the sudden collapse of the interaction for strong shocks once the step preceded the throat. In Figure 17, the strong shock case of $\theta \sim 15°$ was picked to exemplify this sudden collapse. For weaker strength shock the collapse of the interaction was not so sudden and the throat was not so clearly defined.

Interaction Models

Models of the interaction phenomena with varying strength incident shocks are shown in Figure 23. These are based on the combined knowledge obtained from the wall static pressure distribution, the Schlieren and shadow photographs, and the total head survey along the wall.

The interaction can be divided into three basic regimes: 1) A weak incident shock regime, shock strengths below $\theta \sim 7°$ (pressure ratio less than approximately 1.70) where the phenomena is quite similar to the theoretical inviscid case. Here an analysis like Lighthill[4,5] seems quite applicable. The interaction region is of the order of two to three boundary layer thicknesses and no separation occurs. 2) A moderate incident shock regime, shock strengths $8° \leq \theta \leq 12°$ (pressure ratios between 1.75 and 2.30) characterized by a small separated region and the interaction of the incident and reflected shock within the boundary layer. Theoretical

analysis of this regime seems to be quite difficult because of the very strong normal gradients within the boundary layer and the small size of the separated region. 3) A strong incident shock regime, shock strengths above $\theta = 12^{\circ}$ (pressure ratios above approximately 2.3) where the phenomena has spread out to more than ten boundary layer thicknesses and there is an appreciable separated region.

A more detailed model for the 14° shock interaction was obtained in an attempt to shed some additional light on the mechanisms involved for the strong shock interaction with a turbulent boundary layer. Additional total head surveys were made at various distances from the wall and the Mach number distribution throughout the interaction was computed on the basis of constant pressure normal to the wall. These computations are good only near the wall and in the "bifurcated" region where the color Schlieren pictures show little or no normal density gradient. In Figure 24 is presented a schematic drawing of the interaction for the 14° case together with the Mach number contours in the subsonic region. The maximum height of the subsonic and separated regions occur where the incident shocks reflects as from a free jet. At this station the subsonic region is thicker than the boundary layer before the interaction and the height of the separated region is of the order of 1/3 the boundary layer thickness. For this strong shock case, the interaction can be divided into four basic regions for analysis:

(1) The beginning of the interaction, a strong compression region decelerating the flow rapidly and resulting in a doubling of the pressure within a distance of approximately two boundary layer thicknesses.

The flow has not yet separated, mixing probably plays a minor role, and thus this phenomena will probably not be susceptible to the methods of Reference 6.

(2) The start of the separated region and its growth to maximum thickness defines the next region in which mixing probably predominates. The positive but shallow slope of the wall static pressure curve indicated that the mixing rate is increasing over this portion.

(3) The decrease of the separated and subsonic region to the reattachment of the boundary layer occurs in a region of relatively strong adverse pressure gradient. Its slope, as obtained from the wall pressure curve, is roughly four times that of region (2) although only one half as steep as that experienced in region (1). Evidently the concavity of the flow field, the associated centrifugal force, and most probably, a greatly increased mixing rate caused by the shock interaction accounts for this gradient.

(4) Following the reattachment of the boundary layer is a region of slow compression in which the pressure would approach asymtotically the theoretical overall pressure rise if allowed to extend far enough downstream. Were the geometry of the experiment large enough, one would expect the first reflected shock, the following expansion, and the region of slow compression to coalesce to form the single theoretical reflected shock as predicted from inviscid theory.

Regions 2,3, and 4 seem to be quite clearly dominated by the mixing phenomena and should be predictable by an analysis such as Crocco-Lees. The effects of shocks and strong adverse gradients on

mixing rates are, as yet, quite unpredictable and will have to be studied in the various regions.

Corrected Boundary Layer Profiles

In Figure 25 are presented the Mach number profiles at various stations through the 10° interaction. The data utilized for these profiles were the same as presented in Reference 9. It was found that an error had been made in the previous computations. The present computations are based upon the measured wall static pressure assuming constant static pressure normal to the wall. The Mach number distribution shown are, therefore, not correct near the edge of the boundary layer where the presence of shocks and strong normal pressure gradients invalidate the computation. From the profile at station $x = -.7$, the boundary layer ahead of the interaction was found to be fully turbulent in nature, its thickness being approximately .17 inches, the displacement thickness .049 inches, and the momentum thickness .009. The profiles now exhibit a separated region near the zero station substantiating the results found from the total head survey along the wall. In the region of slow compression behind the interaction, (stations $x = .4$ to $+1.6$) the profiles are typical of those in an adverse pressure gradient and, although the wall pressure has reached its maximum and is essentially constant from $x = +.6$ to 1.6, the profiles have not yet filled out to the normal turbulent shape. This seems to indicate that, once reattachment occurs, the mixing rates are roughly those experienced for normal turbulent boundary layers.

GENERAL DISCUSSION

A summary of the wall static pressure distributions are shown in Figure 26. Although the separation data (Figures 20-22) shows an independence of shock strength, the slope of the fore part of the interaction continually decreases from the unseparated case up to a shock strength of $\theta \sim 13^{\circ}$ (pressure ratio of ~ 2.6). Although data at higher shock strengths is not conclusive, the slope appears to be approaching a constant value. The slope of the increasing separated region approaches a constant value for high shock strengths and the reattachment phenomena seems to be relatively insensitive to shock strength. These results lend some weight to the idea of the three regimes previously described.

It has been previously pointed out the the "bump" in the pressure curve and bifurcation of the foot were evidenced only for incident shock strengths of $\theta > 8\frac{1}{2}^{\circ}$ (pressure ratio above 1.7). Page and Sargant[8] in their tests at Mach numbers of 1.2 to 1.6 found that bifurcation of normal and oblique shocks always occurred when the incident shock pressure ratios were greater than 1.65. An examination of the results of Bardsley & Mair[7] show a similar result at a Mach number of about 2. It therefore appears that the beginning of the bifurcation (forward propagation of the interaction by separation) is not a strong function of Mach number, indicating that the supersonic portion of the boundary layer is not playing a significant part in the phenomena. The effect of thickness of the subsonic region can also be eliminated since the relative extent of the subsonic region varies considerably over the range of Mach numbers examined, 1.2 to 3.0.

The effect of incident shock pressure ratio on the length of the interaction and separated regions is summarized in Figure 27. These results were compared to those of Gadd, Holder, and Regan[10] and show disturbing discrepancies. The influence region, defined as the distance from the zero point to the start of the interaction expressed in nondimensional units, was found to be only half that of Reference 9. In addition, the shape of the curve was considerably different, approaching some constant value rather than increasing precipitously. Reference 9 predicts a wall static pressure ratio of approximately 2.4 at separation and is checked by their experiments. The results reported herein give a value of 2.0. The discrepancies are far outside the experimental accuracy but may be explainable by the fact that full span shock generators were not used in the work of Reference 9.

CONCLUSIONS

The results of the present investigation may be summarized as follows:

1. It is quite important that all experiments on shock wave boundary layer interactions be carefully checked for two-dimensionality. Shock generators which do not completely span the tunnel and weak shock interactions may exhibit serious cross flow phenomena. These may explain some of the discrepancies in existing data.

2. Below an incident shock pressure ratio of ~ 1.7, the interaction is similar to the theoretical inviscid case. The incident shock is reflected as a single compression, no separation exists, and the pressure rise on the wall is smooth and completed in about two to three boundary layer thicknesses.

3. Slightly above an incident shock pressure ratio of 1.7, the wall static pressures exhibit a "bump", bifurcation of the incident shock occurs, and the reflection changes to a compression, expansion, compression region. This indicates the onset of separation. The incident shock pressure ratio for separation appears to be practically independent of Mach number of the basis of the results presented herein and those of Bardsley and Mair and Fage and Sargant.

4. For incident shock strengths above 1.75, separation occurs about two boundary layer thicknesses from the beginning of the interaction at a wall static pressure ratio of $\sim$ 2.0. This phenomena is independent of shock pressure ratio over the range tested.

5. Between incident shock pressure ratios of 1.75 to 2.30, the interaction is characterized by a small separated region, and the interaction of the incident and reflected shock within the boundary layer.

6. For incident shocks of pressure ratios above 2.3, the interaction spreads to more than ten boundary layer thicknesses and there is a large separated region. To the first order, increased shock strength changes the scale of the interaction region without changing its structure. The various region of the interaction are separated sufficiently for detailed study.

7. There are considerable discrepancies between the data presented herein and those presented in Reference 10. This may be due in part to the span of the wedges used by the latter investigators.

REFERENCES

1) Leipmann, H.W., Roshko, A. and Dhawan, S.: On the Reflection of Shock Waves from Boundary Layers. NACA TN 2334, April 1951.

2) Barry, F.W., Shapiro, S.H., and Newmann, E.P.: The Interaction of Shock Waves with Boundary Layers on a Flat Surface. Meteor Report No. 52, Massachusetts Institute of Technology, March 1950.

3) Lees, L.: Interaction Between the Laminar Boundary Layer Over a Plane Surface and an Incident Oblique Shock Wave. Princeton University Aeronautical Engineering Department Report No. 143, January 1949.

4) Lighthill, M.J.: On Boundary Layers and Upstream Influence; Part I: A Comparison Between Subsonic and Supersonic Flows. Proceedings of the Royal Society, Volume 217, 1953.

5) Lighthill, M.J.: On Boundary Layers and Upstream Influence; Part II: Supersonic Flows with Separation. Proceedings of the Royal Society, Volume 217, 1953.

6) Crocco, L. and Lees, L.: A Mixing Theory for the Interaction Between Dissipative Flows and Nearly-Isentropic Streams. Princeton University Aeronautical Engineering Department Report no. 187, January 1952.

7) Bardsley, O. and Mair, W.A.: The Interaction Between an Oblique Shock Wave and a Turbulent Boundary Layer. Philosophical Magazine, Series 7, Volume 42, January 1951.

8) Page, A. and Sargant, R.E.: Shock Wave and Boundary Layer Phenomena Near a Flat Surface. Proceedings of the Royal Society, Volume 190, Series A, No. 1020, June 1947.

9) Bogdonoff, S.M. and Solarski, A.H.: A Preliminary Investigation of a Shock Wave-Turbulent Boundary Layer Interaction. Princeton University Aeronautical Engineering Department Report No. 184, 1951.

10) Gadd, G.E., Holder, D.W., and Regan, J.D.: The Interaction of an Oblique Shock Wave with the Boundary Layer on a Flat Plate; Part II: Interim Note on the Results for M = 1.5, 2, 3, and 4. British A.R.C. 15,591 (unpublished)

11) Bogdonoff, S.M.: The Princeton Pilot Variable Density Supersonic Wind Tunnel. U.S. Navy Project Squid, Technical Memorandum, No. PR-8. Princeton University, May 1948.

APPENDIX A

COLOR SCHLIEREN SYSTEM

Schlieren photography has proven to be one of the major tools of the experimental engineer. Although the Schlieren system is sensitive to density gradients, it provides only a qualitative picture. Some efforts have been made to get quantitative data, but with little success. One of the drawbacks has been the fact that the eye is not very sensitive to the gray scale. For accurate matching of grays in different parts of a single photograph, photo-electronic techniques must be used.

In an attempt to get a photograph which was easier to examine in detail by eye, and perhaps adaptable to quantitative studies, a color Schlieren system was set up. The use of color Schlieren is not new and several color photographs have been published over the years. To the best of the authors' knowledge, all these pictures were taken with relatively long exposures because of the slowness of the color film. These long exposures, while producing the desired colorful pictures, made the method unusable as a research tool because of the "smearing out" of the fine detail caused by slight oscillations. With the rather conventional system used in the present investigation and the special film processing described in Appendix B, high quality color Schlieren photographs have been taken with exposure time of the order of one microsecond.

The final photograph is one in which a density gradient is distinguished by a particular color and the system can be so adjusted to give all or part of the spectrum for any desired range of gradients. For example, a boundary layer can be made to be seen as going from green at the outer edge, through yellow and orange to red at the wall.

The color technique has been particularly useful when there are strong interactions of compression and expansion waves, boundary layers and separated regions. For such cases, the system provides high sensitivity without overloading troubles.

The optical apparatus used was an adaptation of the conventional two mirror system (see figure below). The changes consisted of, 1) the use of a "line" spectrum of light instead of a point source at the focal point of mirror A, and 2) the replacement of the knife edge at the focal point of mirror B with one adjustable slit to permit the selection of background color and sensitivity.

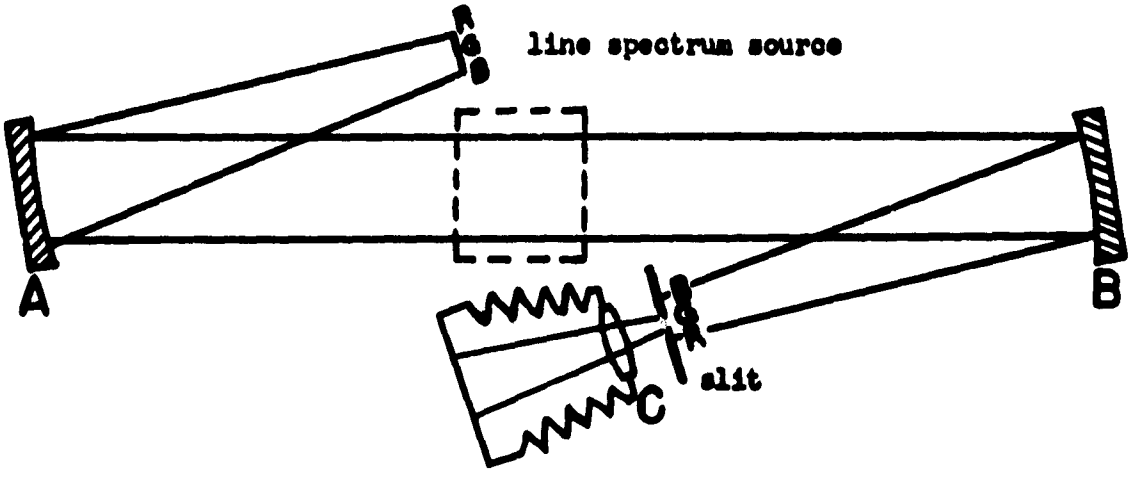

The two spherical concave mirrors, A and B, had a focal length of 100 inches and a diameter of 12 inches. The objective lens, D, is an achromat of 9 3/4 inches focal length. This resulted in an image approximately 1/10 the size of the object which was necessary to obtain a strong enough concentration of light to expose the film.

The light source was a high pressure spark consisting of two steel conical electrodes separated by a lucite spacer. Maximum light was obtained by using a 3/32" orifice in one electrode and a 3/32" hole through the lucite spacer. The discharge of a .25 MFD oil filled condenser, charged to approximately 15 KV, across the above spark gave a satisfactory film exposure in about one microsecond. Condenser lense L_1 was used to produce parallel light which was passed through a direct view prism, and lens L_2 converged the light to produce the line spectrum.

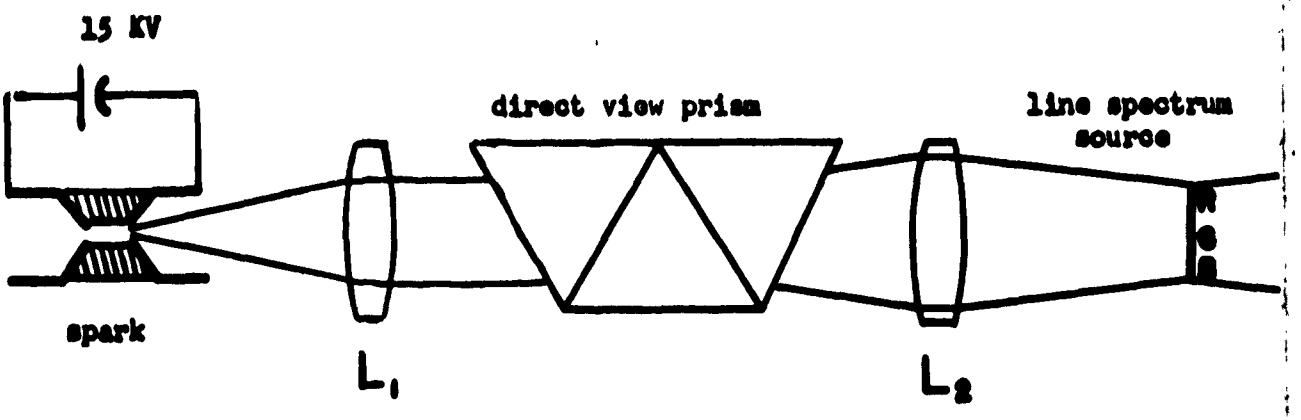

The divergence of the prism and the focal length of lense L_2 determined the spread of the line spectrum. In the apparatus used, the spread of the spectrum was approximately 3/4 inches. It should not be felt that use of a direct view prism is mandatory. A regular prism, a constant deviation prism, or a coarse diffraction grating could be used equally well to obtain the desired line spectrum. Depending on the tunnel size, density level, and phenomena to be studied, the length of the spectral line and width of the slit can be adjusted to give the full spectral spread.

Once a satisfactory color photograph or transparency has been obtained, it seems quite possible to obtain some quantitative data. If the color transparency is printed on a single sheet of ordinary developing paper (black and white) by successively exposing through a series of narrow color filters, a pattern of lines will be obtained. Each line is made by the light of a particular narrow frequency range (color) determined by the filter. The resulting photograph would be similar to an interferogram except that its lines would be of constant gradient rather than constant density. An undisturbed boundary layer or a lense in the optical field could provide a calibration curve. These possibilities are presently being investigated. They include, however, the small optical difficulties of being integrating machines and susceptible to diffraction and non two-dimensionality errors. The corrections applied to interferograms must also be used here.

APPENDIX B

COLOR FILM PROCESSING

Sylvester Hight

In working with a color Schlieren system, one is immediately confronted with the problem of light, both as to quality and quantity. In its use for investigating the boundary layer phenomena under consideration, the exposure time must be of the order of one to two microseconds. In order to obtain exposures of this short duration, a spark is the logical choice.(Appendix A) Although this source did not produce enough light to give a properly exposed picture, it at least was close enough so that further manipulation of the photographic phase was able to produce the desired results.

There are available several films which can be used to produce color transparencies. They are Ektachrome, Ansco-Color, and Kodachrome. Kodachrome would be the ideal choice were it not for the fact that the illumination was of threshold value. This would require special developing techniques which could not easily be applied by the Eastman Kodak processing plants. This, plus the delay that would be involved in the transportation of the exposed materials to and from the processing laboratory, dictated the choice of Ektachrome sheets which could be processed immediately in the available darkroom. This particular film shows a very long scale with good gradations of color and fairly wide latitude.

The film is available in both daylight and indoor balance. On first assumption, it would seem that daylight film would be the logical choice since the spark source used emits a light that is visually quite blue and approaching daylight in quality. Actual experiment, however, indicated

that indoor type film, with its greater blue sensitivity, gave the desired results without the concomitant darkening and degradation of the blues in the picture. This is, apparently, a manifestation of the reciprocity law failure. One would expect the effect to be greater on the panchromatic sensitized layer which is ultimately the producer of the cyan dye image. It should also be a function of the color of the original light source. This is due to the fact that the blue in the spectrum is spread out more then the other colors, thereby reducing the intensity per unit area.

In the course of trying to increase the sensitivity of the system, several systems were tried to increase the speed of the film. Hypersensitisation with mercury vapor was used along with increased developing time. Both methods can be used, but caution must be exercised to see that they are not overdone. Hypersensitisation produced the greater increase in speed but had to be carefully controlled since it also produced the undesirable result of desaturating the blacks and the colors. It was found that hypersensitisation for a period of 12 hours was about maximum and even for such a short period there was marked desaturation present. Much longer periods in the mercury vapor gave results that were entirely unusable.

Longer developing times, in the long run, proved to be the most profitable course to follow. In normal usage, Ektachrome film can be developed in about an hour. The first step would be to develop in the first developer for about ten minutes. This results in a black and white negative image. The film is then rinsed and placed in the hardener bath for three

to ten minutes. After three minutes in the hardener, which also acts as a stopbath, the room lights can be turned on. The balance of the procedure is then carried on under full illumination. The film, at this point, is exposed to the light of a photoflood lamp for five seconds per side at a distance of one foot. This is to completely expose any remaining undeveloped silver halide in the three layers. From this point the color developing is continued as per instructions.

With the spark and optical set-up used, first developer times had to be increased to the order of 13 to 21 minutes. Times of this order did not appreciably alter the color balance of the picture and maintained good background saturation. This was the only time that had to be changed, since the increased developing at this stage resulted in increased contrast density of the original negative image. This gave a positive which was lighter and more normal in appearance. If still more increase in speed were necessary, it would be possible to decrease the time of the reversal exposure and continue the processing in the dark. The result of this would be to give a fairly normal appearing positive despite the very weak negative image on the film. It was felt, however, that since perfect results could be obtained merely by increasing development time slightly, any resulting benefit from decreasing re-exposure time would be more than offset by the difficulty of maintaining proper temperatures and manipulating films in the dark.

The films were all developed in a tray by shuffling constantly in all of the solutions. During the development procedure, each film was lifted completely out of the developing solution in order to permit aerial

oxidation each time it was handled. This resulted in an appreciable increase in density (in the negative image) without a correspondingly great increase in developing time.

It should be mentioned in passing that one will encounter quite a bit a variation in producing color pictures for several reasons. First, color film is not constant in response from one batch to another. It would be advantageous to purchase enough film of the same emulsion number to complete a series of photographs. Secondly; the spark does not deliver a constant output from day to day or from picture to picture due partly to atmospheric conditions. The variations within a particular sequence are usually not great enough to ruin the set. This instability of the spark is accentuated by increasing the developing time, which raises the slope of the film's characteristic curve. For these reasons, it was found convenient to make several dummy pictures right after the regular series was completed. These dummies were developed for varying times and from these results, the best time was determined for the developing of the test set. With a good deal of experience, a skilled operator might be able to judge proper timing from the density of the negative image just before re-exposure. However, the determination of final color balance cannot be made this way. Once a satisfactory black and white negative has been obtained, the remainder of the color developing procedure is normal.

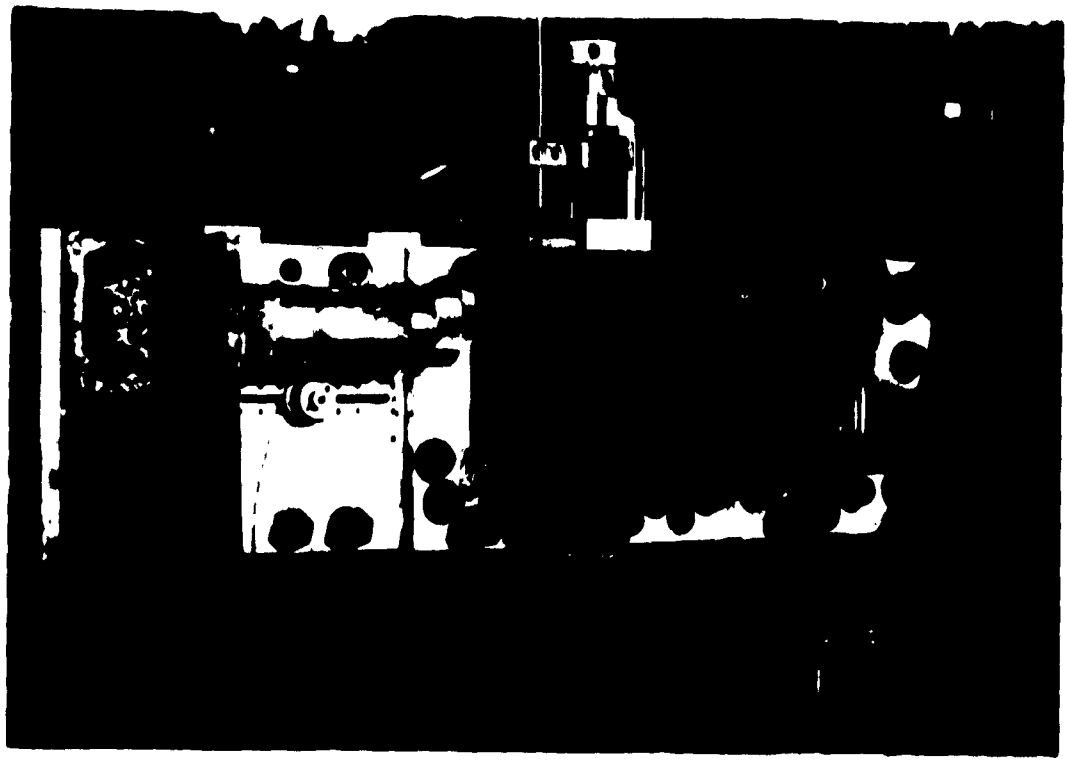

Figure 1 Experimental Installation in Wind Tunnel; Showing Shock Generator, Total Head Probe, and Micrometer Drive systems for Wedge and Probe.

Figure 2 Shock Generators; Showing mounting and angle changing mechanisms.

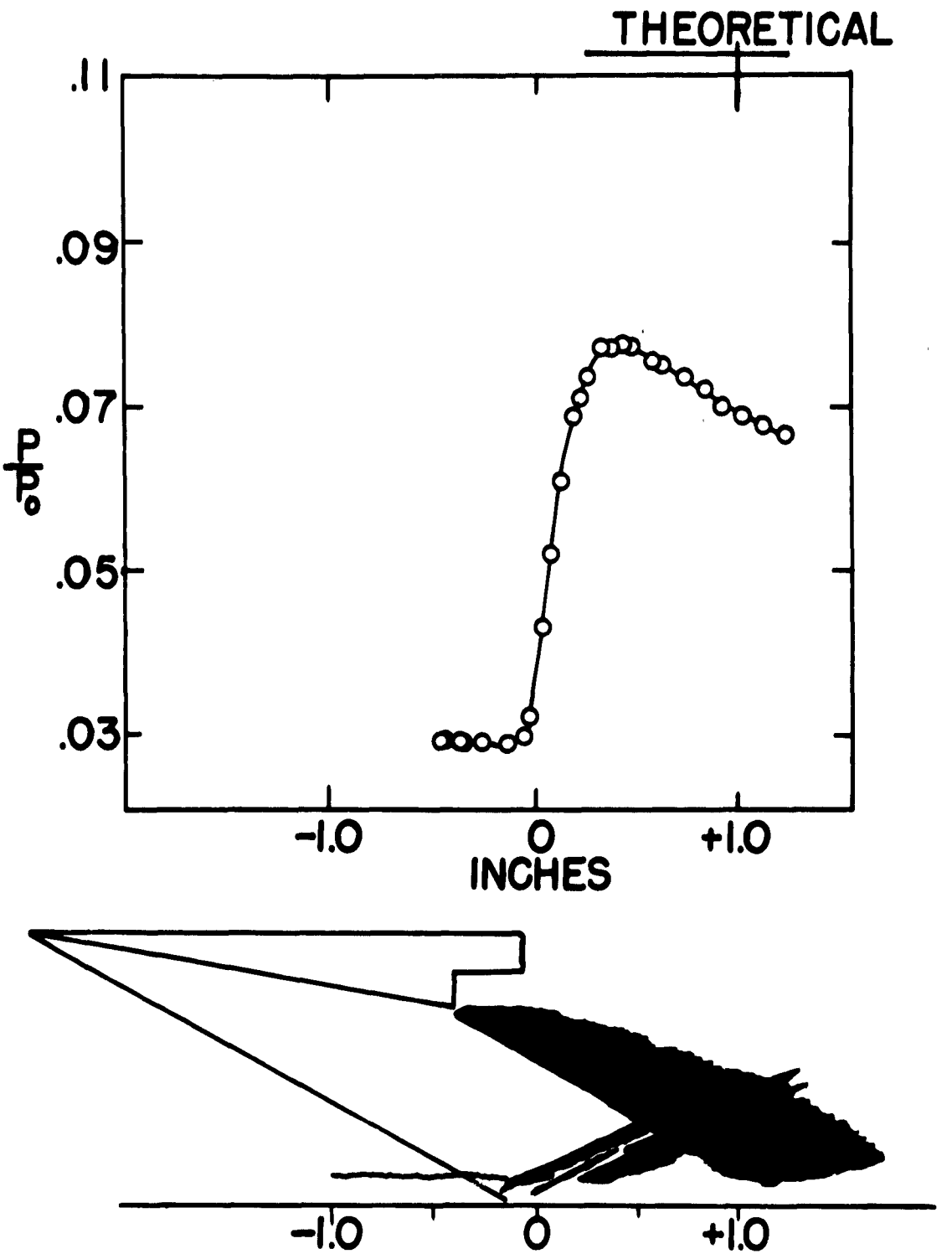

Figure 3 Sketch of Interaction and Wall Static Pressure Distribution for Narrow Wedge

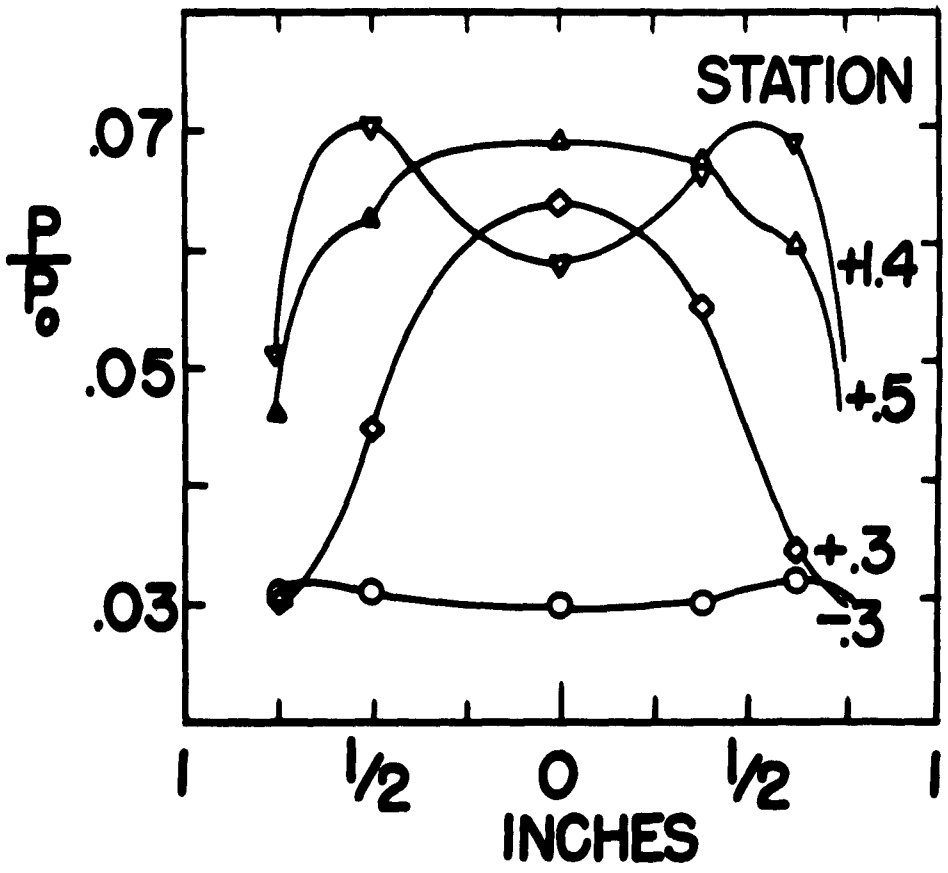

Figure 4 Spanwise Static Pressure Distribution for Several Shock Positions for Narrow Wedge

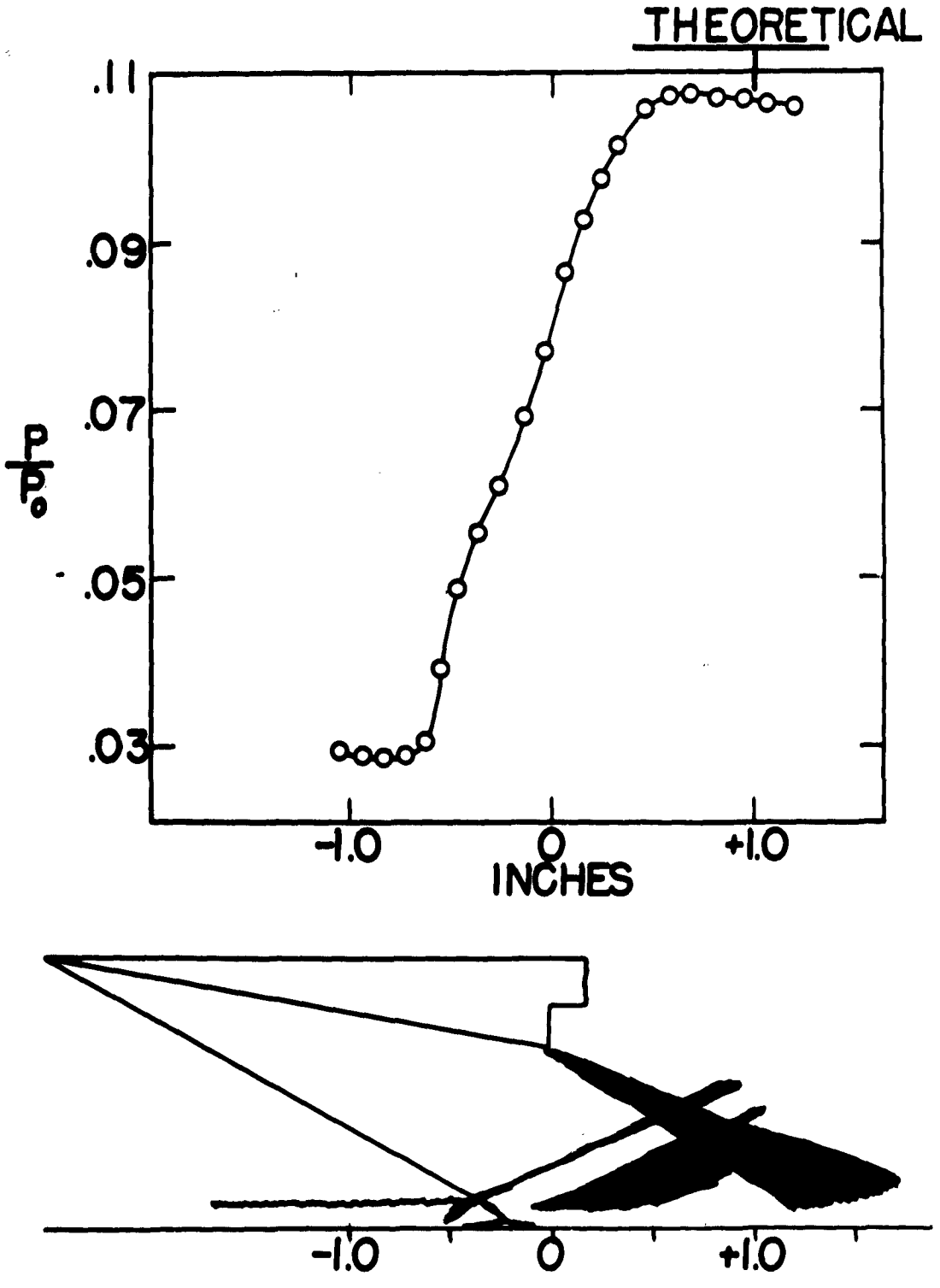

Figure 5 Sketch of Interaction and Wall Static Pressure Distribution for Full Span Wedge

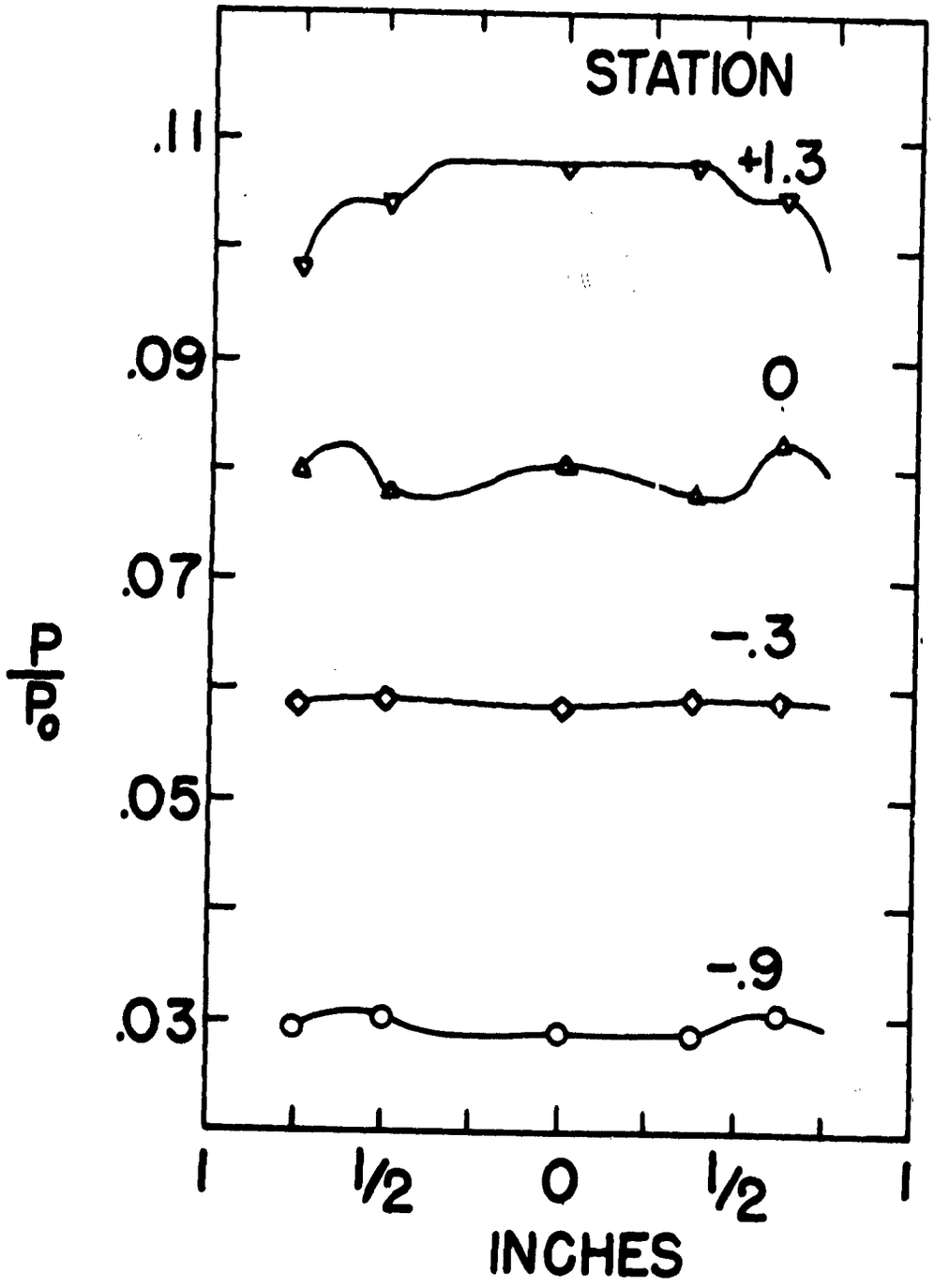

Figure 6 Spanwise Static Pressure Distribution for Several Shock Positions for Full Span Wedge

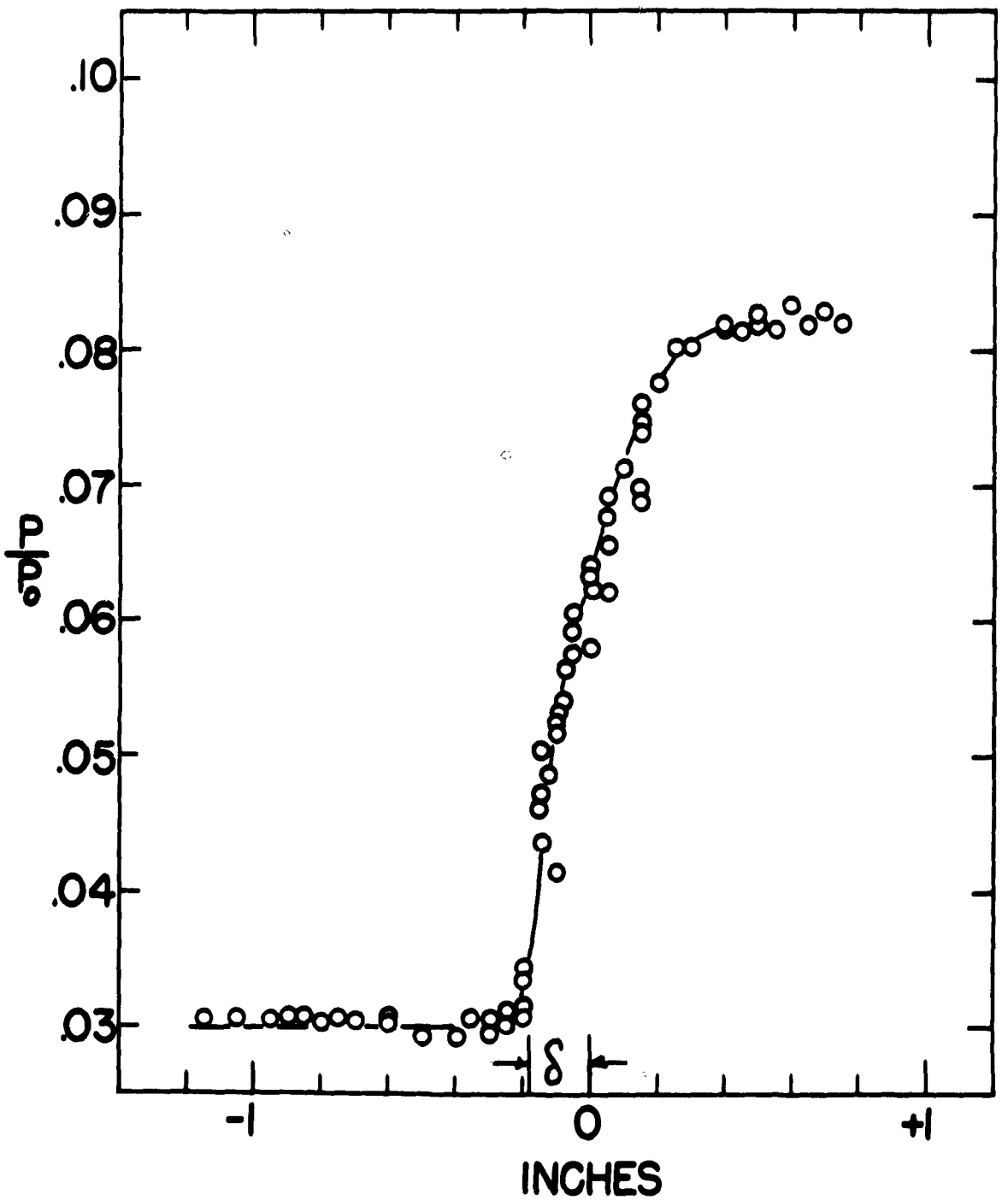

Figure 7 Wall Static Pressure Distribution for 7° Shock

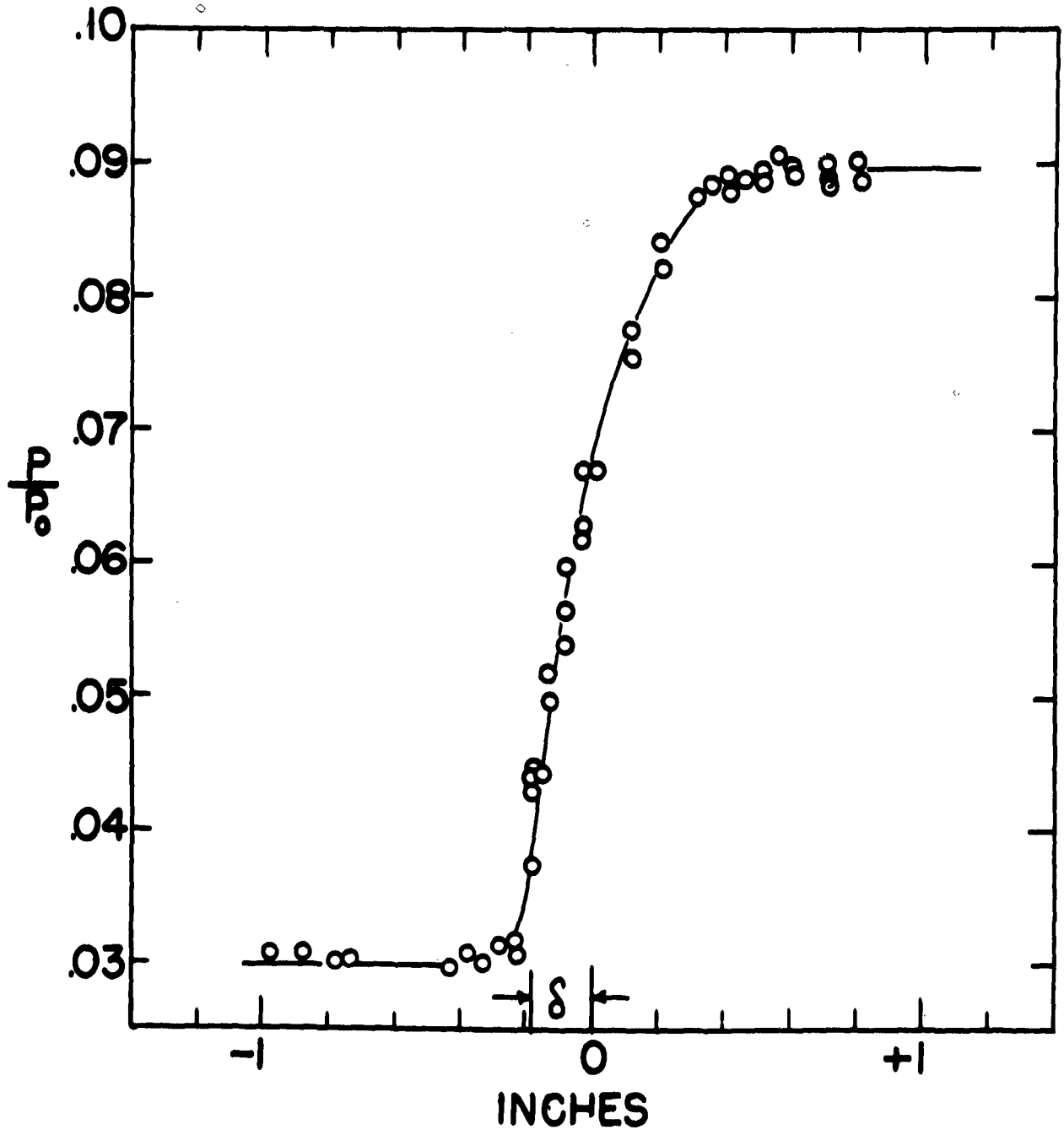

Figure 8 Wall Static Pressure Distribution for 8° Shock

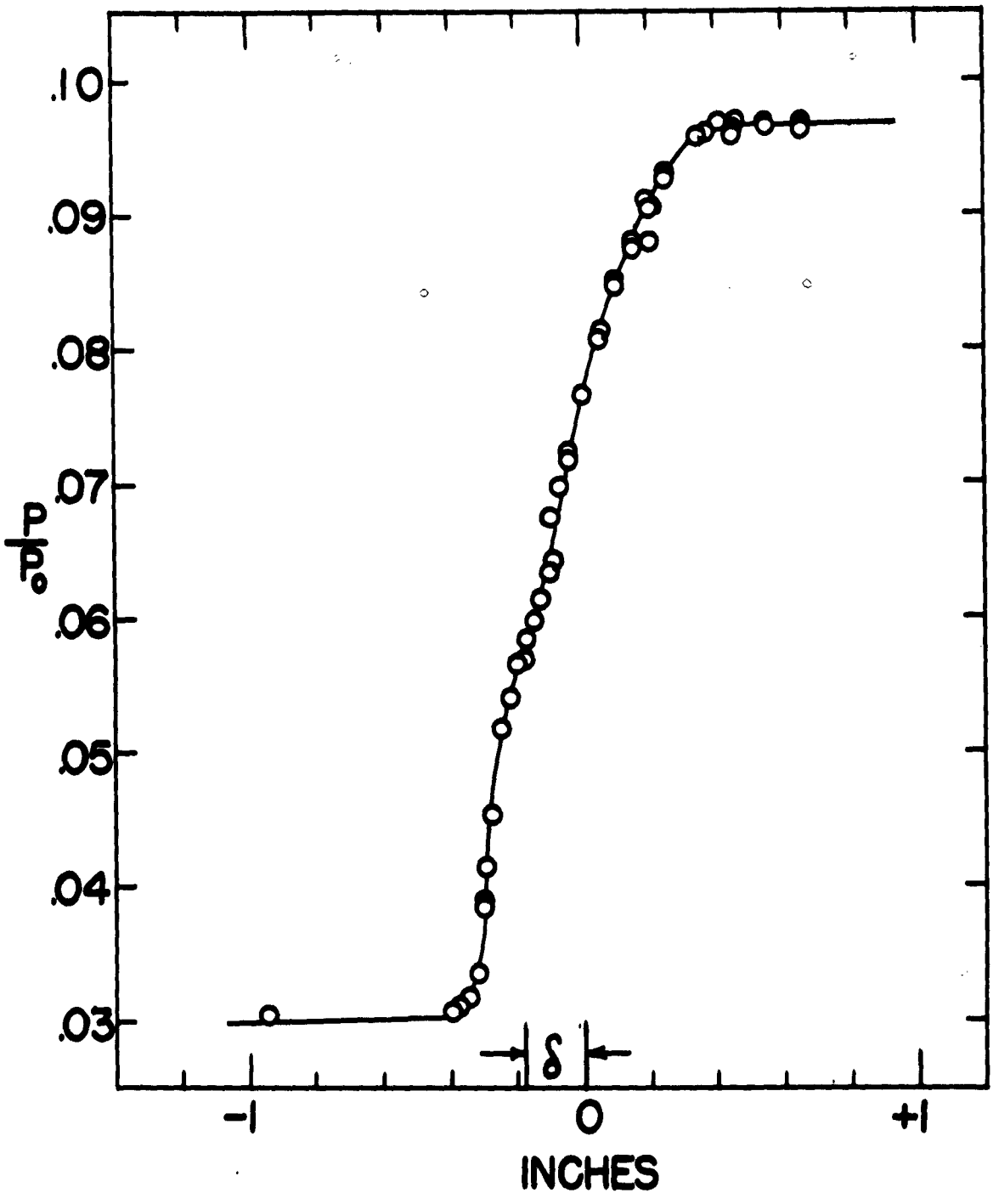

Figure 9 Wall Static Pressure Distribution for 9° Shock

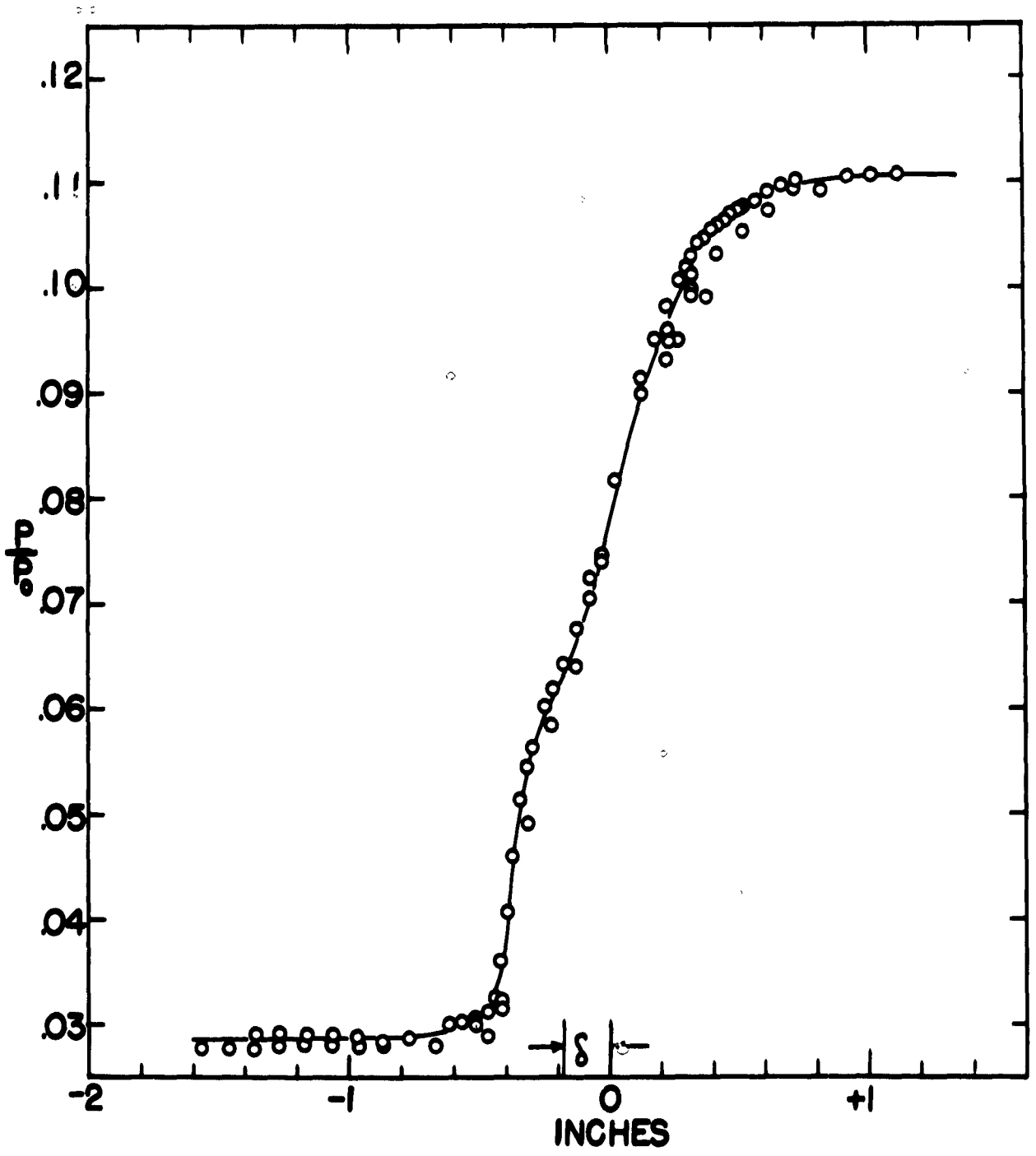

Figure 10 Wall Static Pressure Distribution for 10° Shock

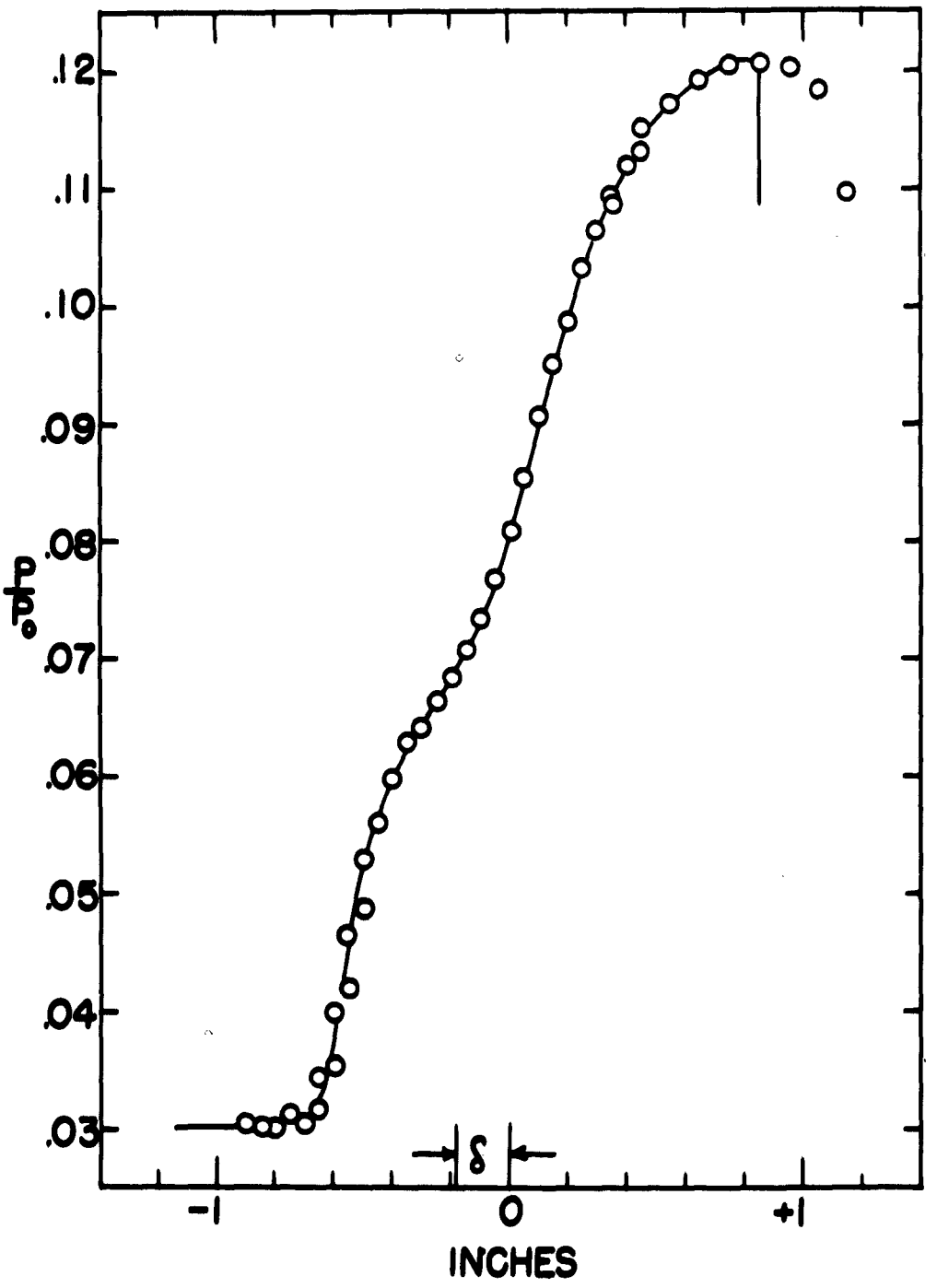

Figure 11 Wall Static Pressure Distribution for 11° Shock

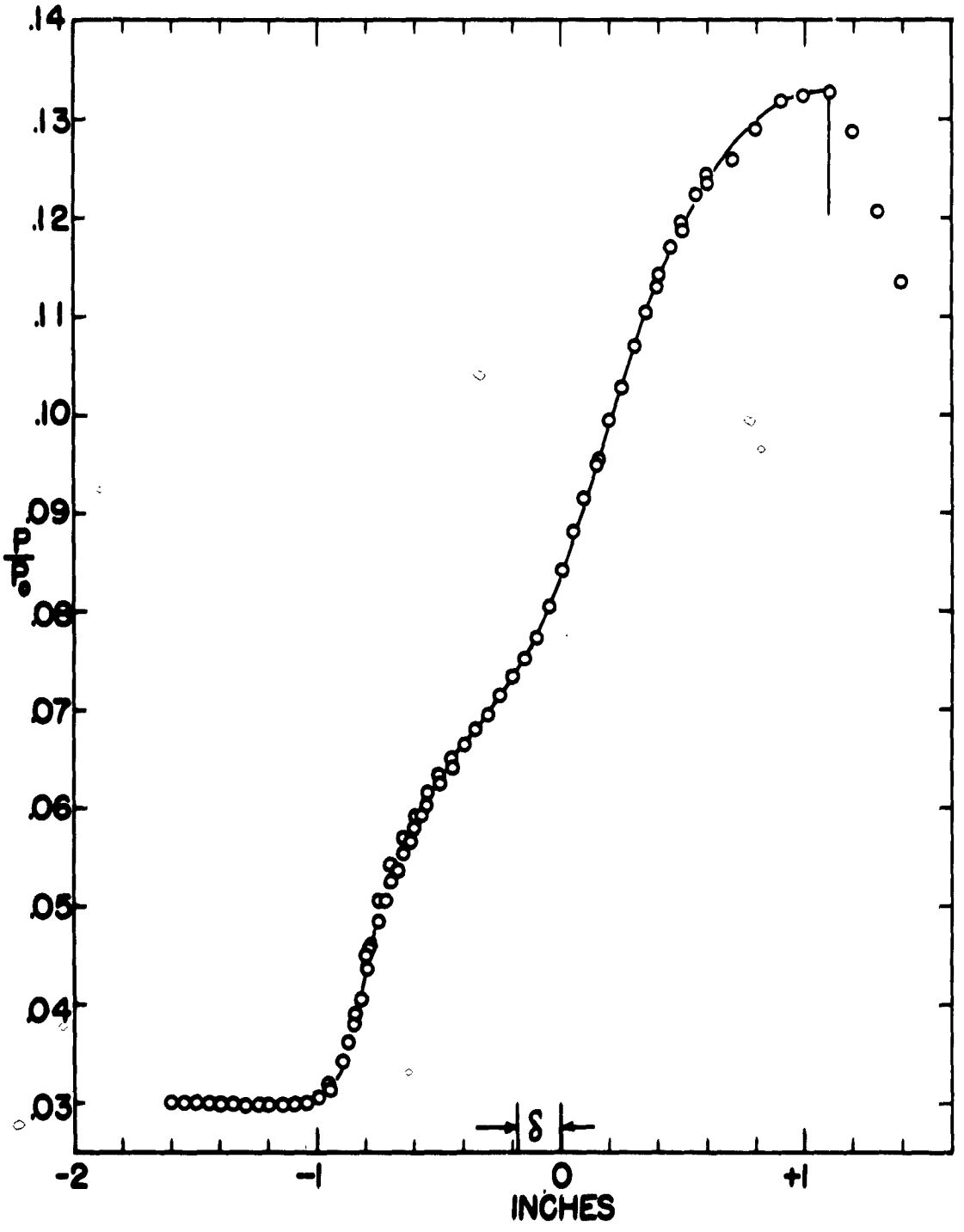

Figure 12 Wall Static Pressure Distribution for 12° Shock

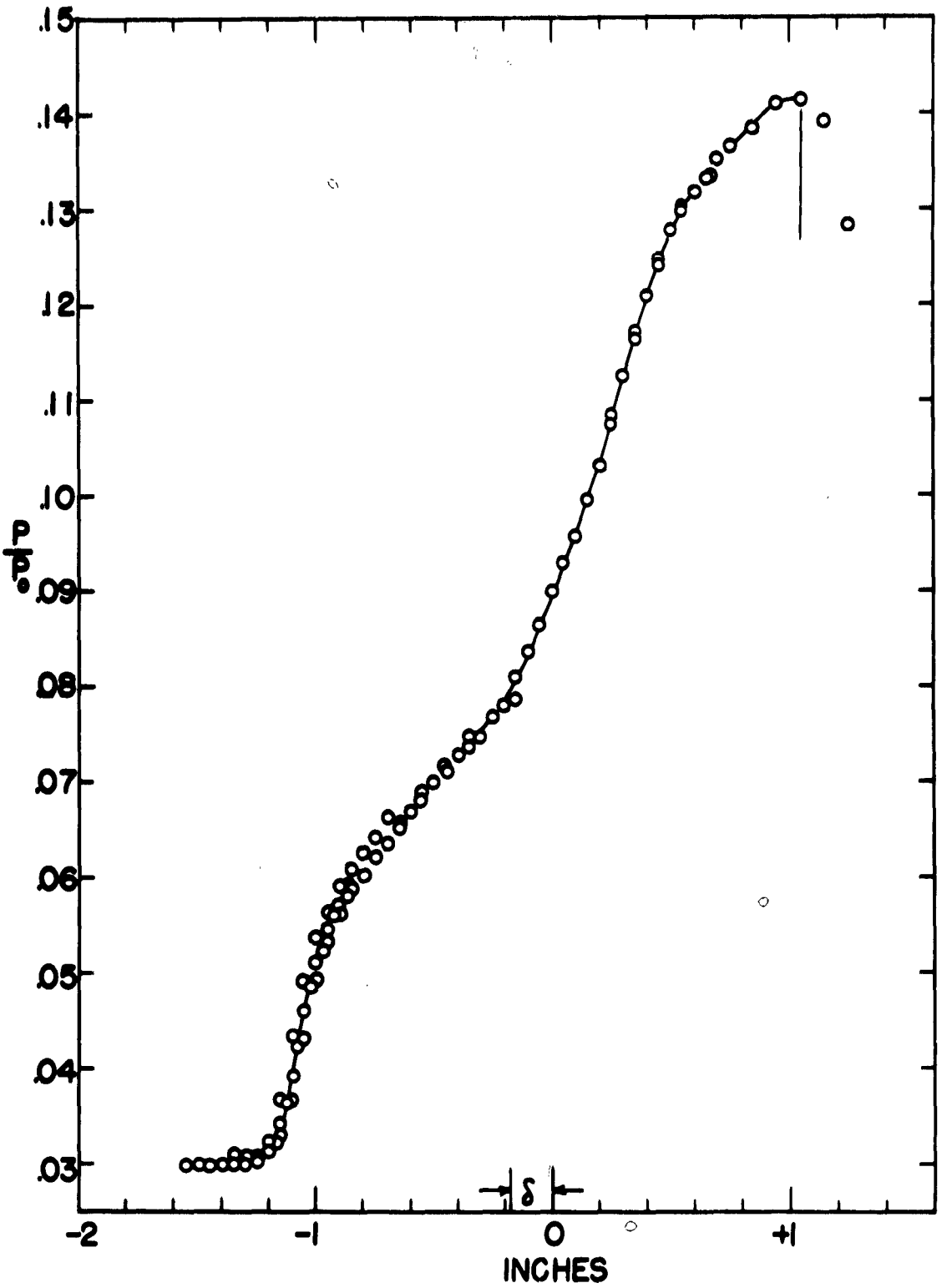

Figure 13 Wall Static Pressure Distribution for 13° Shock

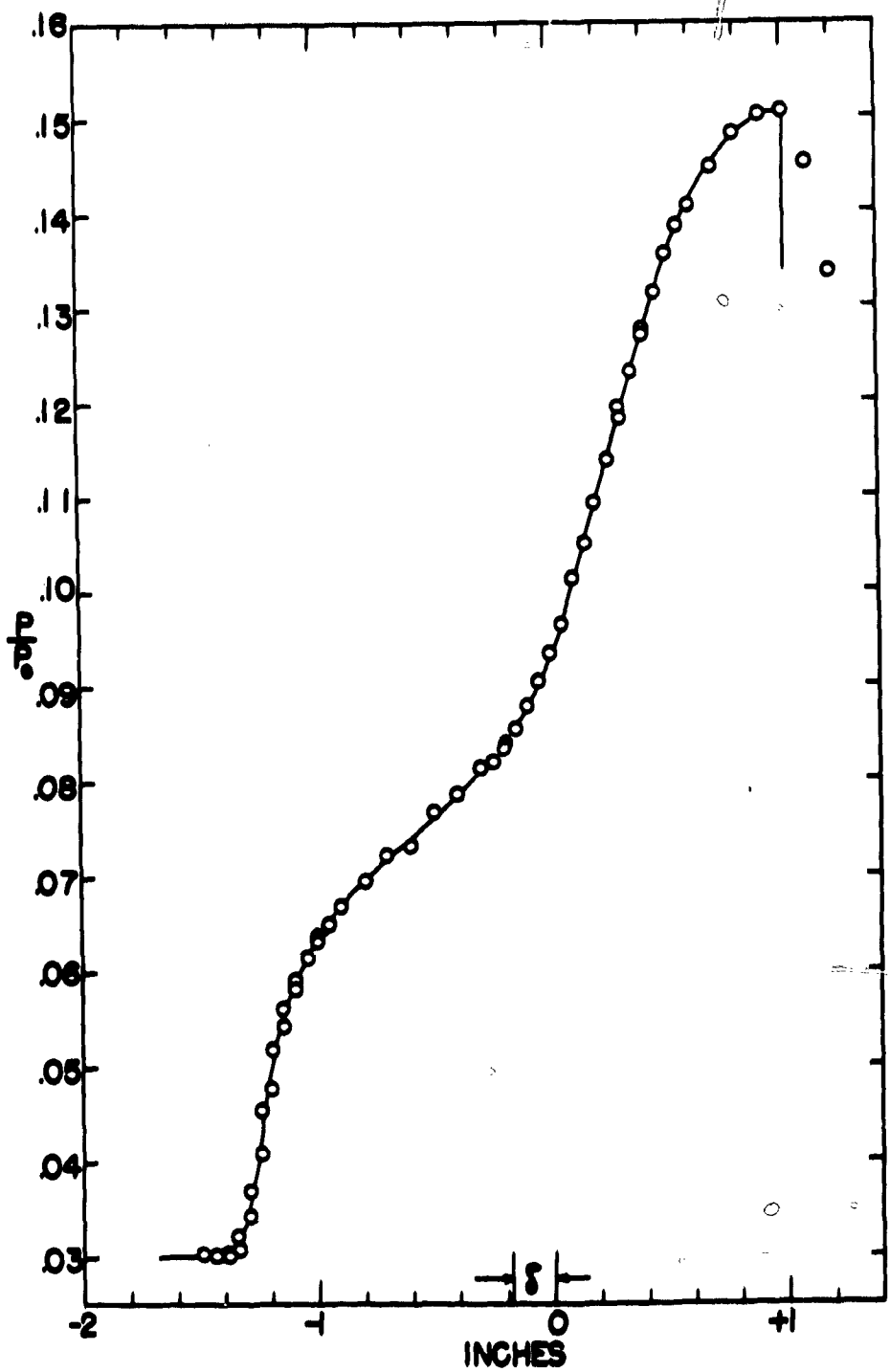

Figure 14 Wall Static Pressure Distribution for 14° Shock

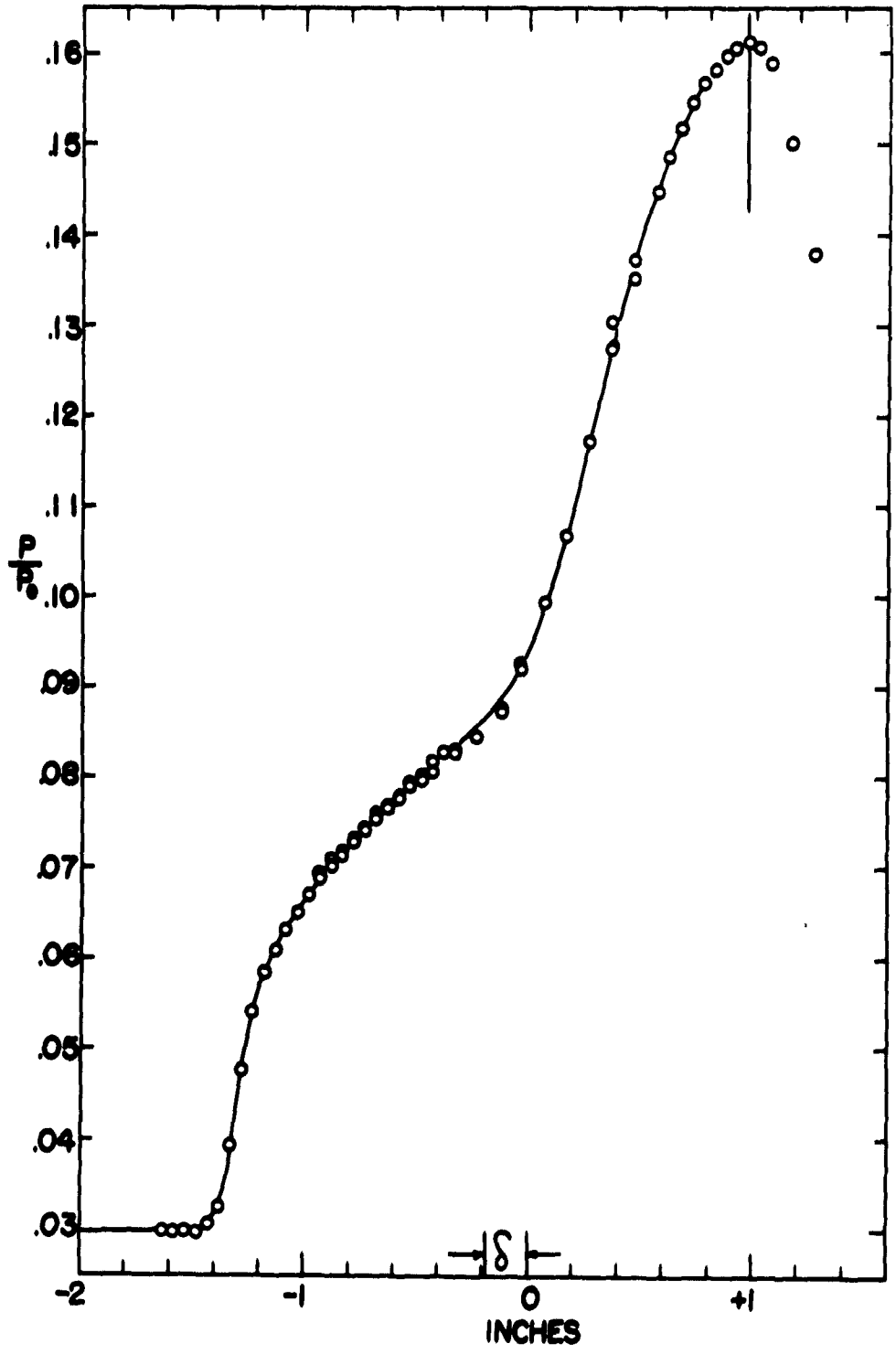

Figure 15 Wall Static Pressure Distribution for 15° Shock

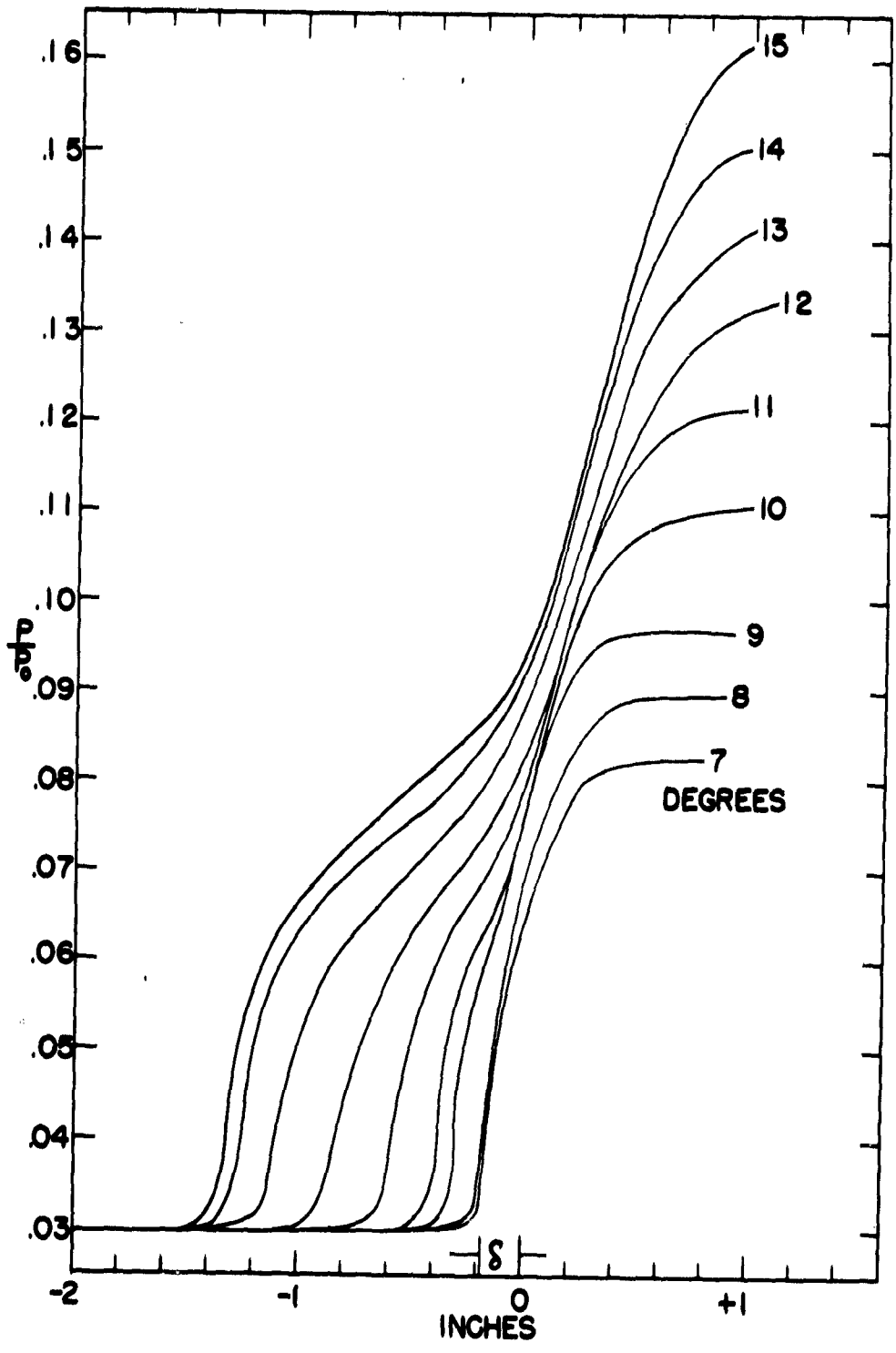

Figure 16 Wall Static Pressure Distribution for All Strength Shocks

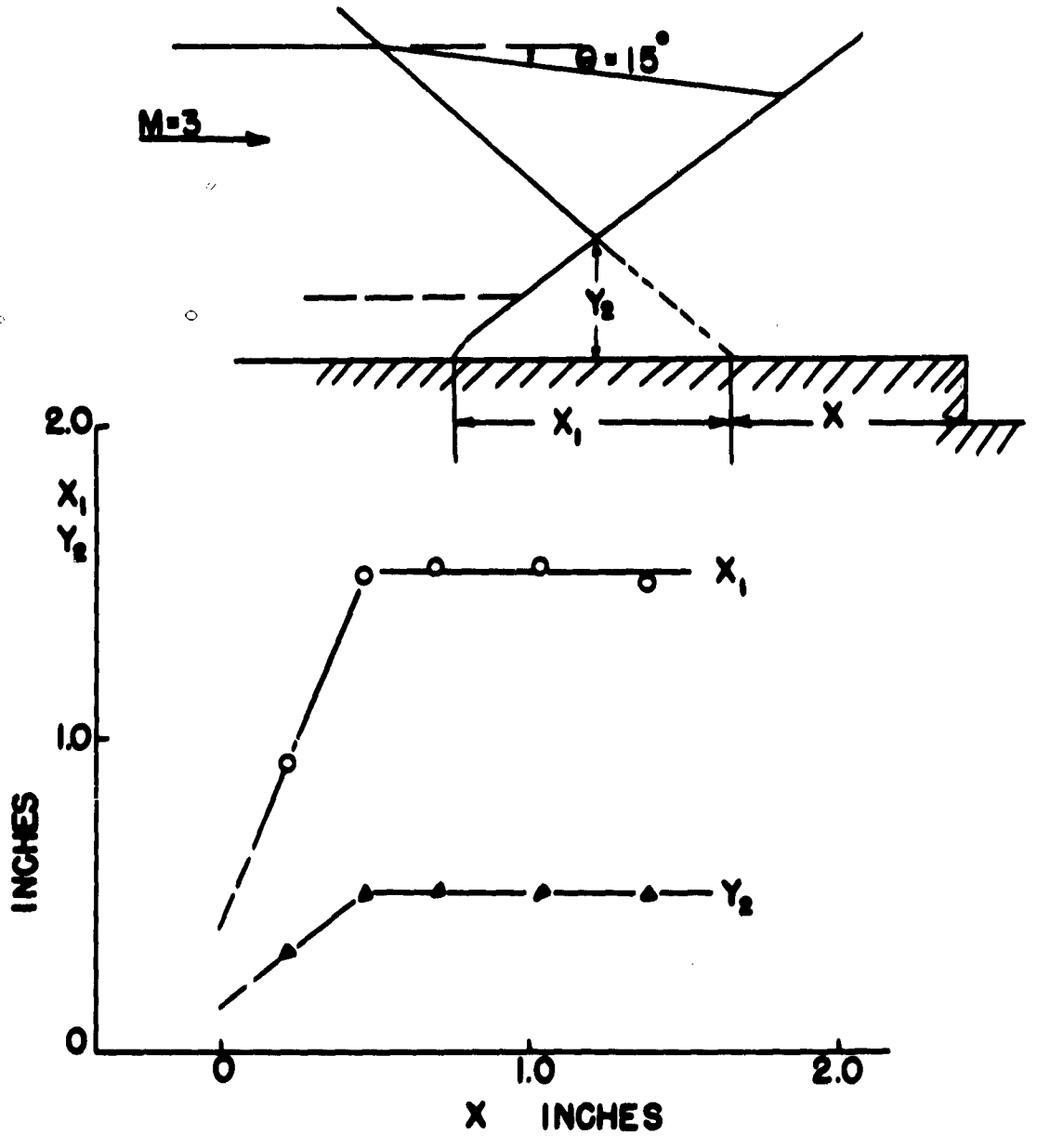

Figure 17 Effect of Downstream Disturbances on Interaction

θ = 7

θ = 8

θ = 9

Figure 18 Optical Studies of the Interaction of Varying Strength Shock Waves with Turbulent Boundary Layer Schlieren Photographs (Horizontal Cut-off)

θ = 10

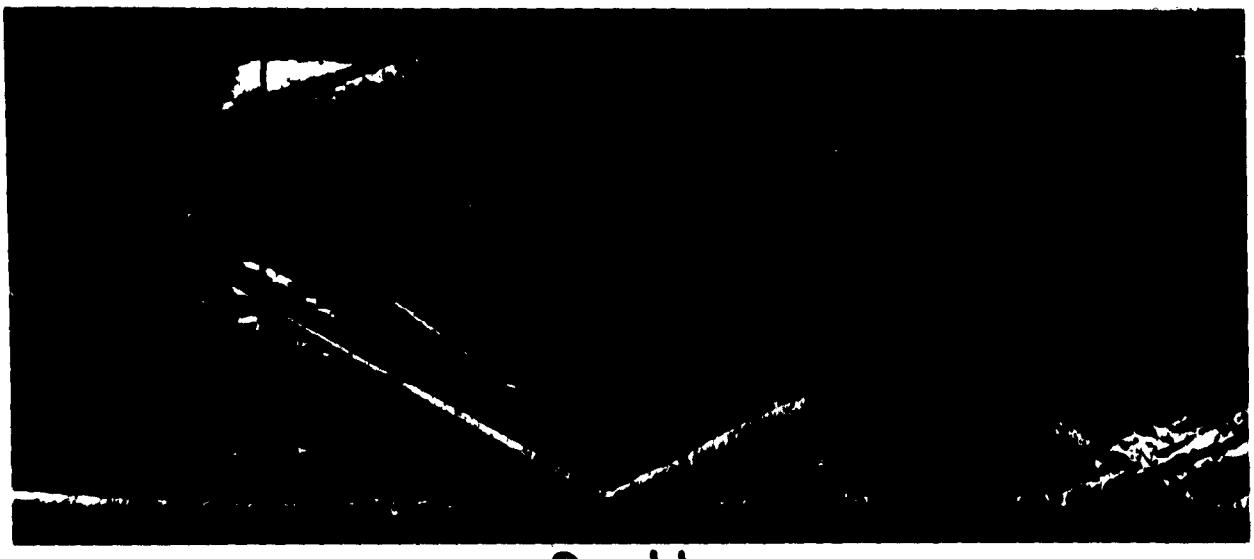

θ = 11

θ = 12

Figure 16 Continued Schlieren Photographs (Horizontal Cut-off)

θ = 13

θ = 14

θ = 15

Figure 18 Continued Schlieren Photographs (Horizontal Cut-off)

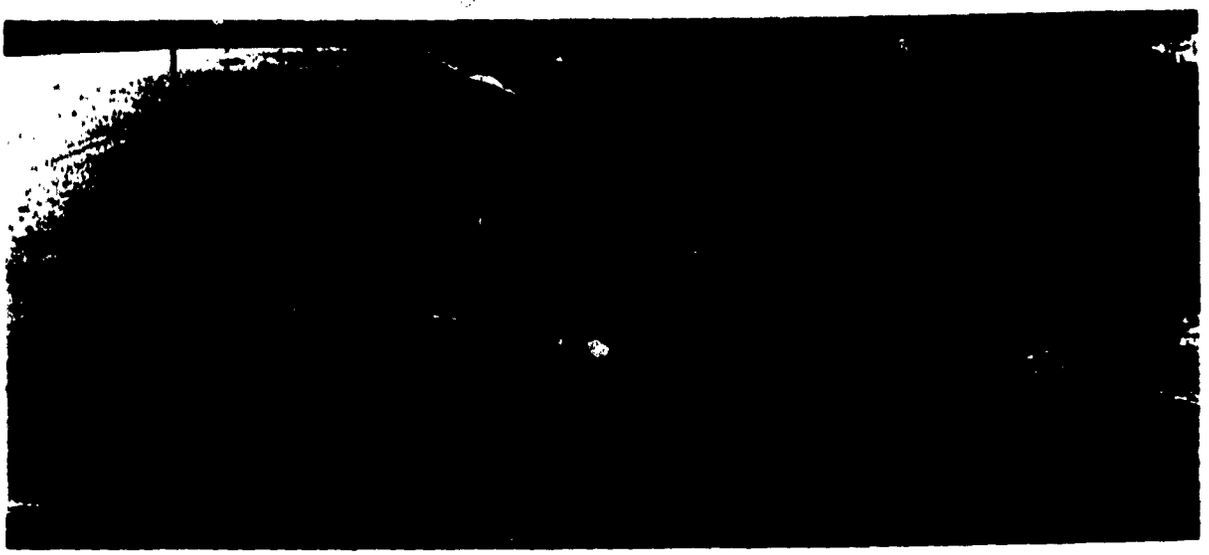

θ = 7

θ = 8

θ = 9

Figure 18 Continued Shadowgraphs

θ = 10

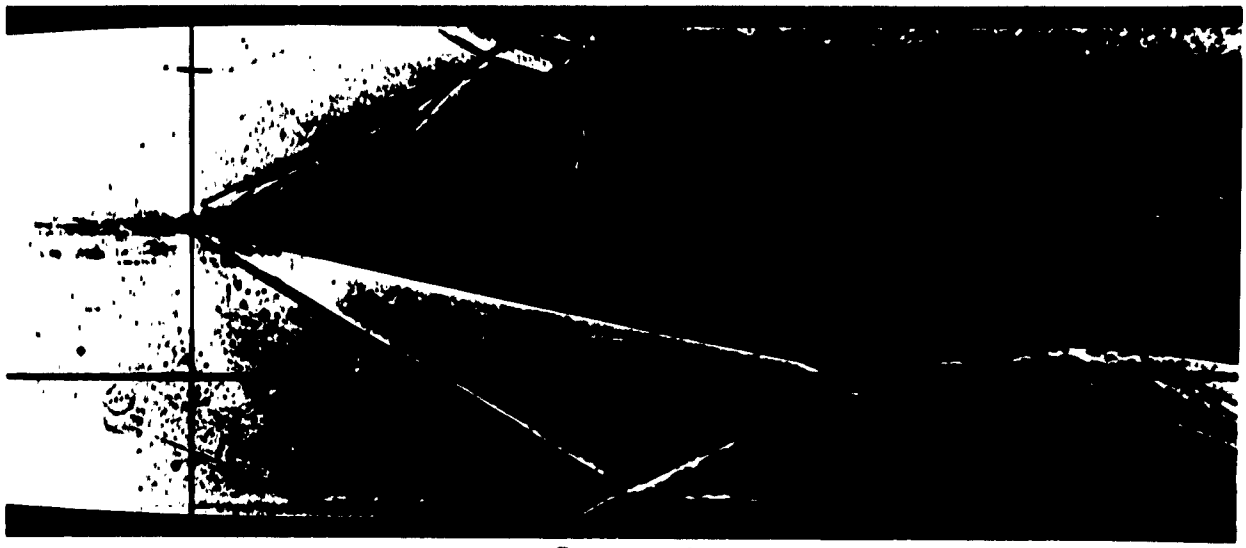

θ = 11

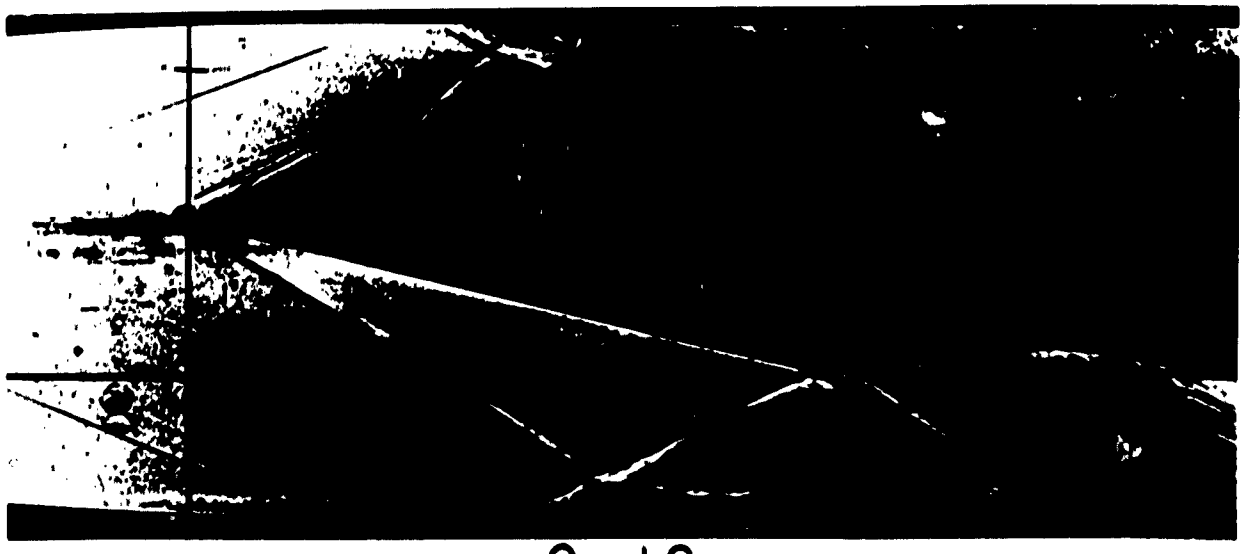

θ = 12

Figure 13 Continued Shadowgraphs

θ = 13

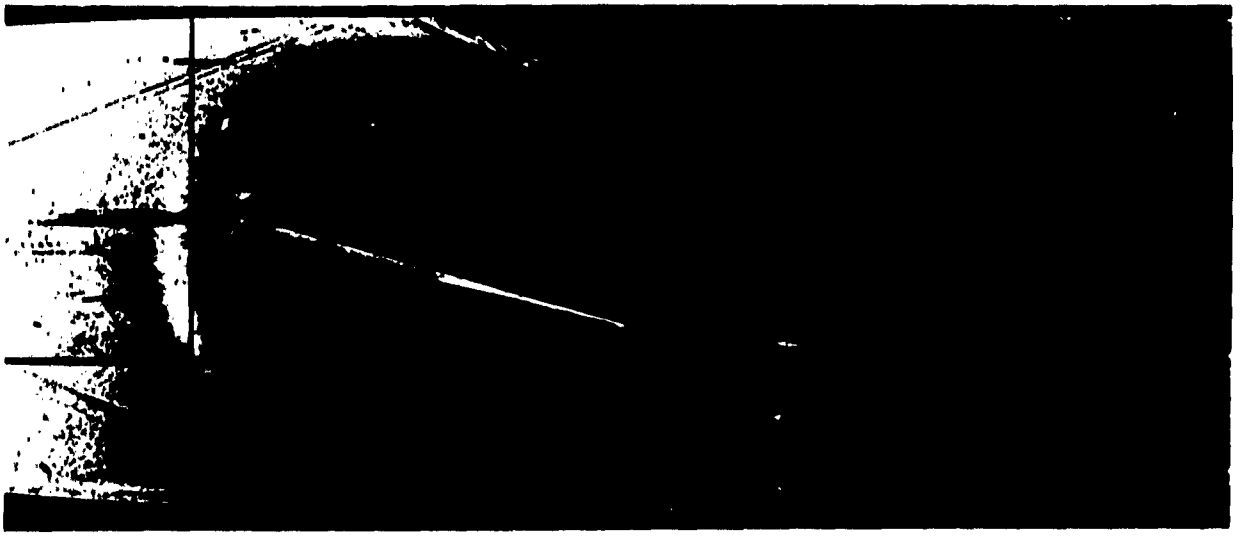

θ = 14

θ = 15

Figure 15 Included Shadowgraphs

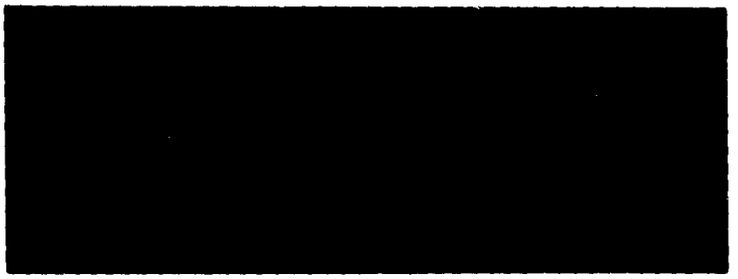

Figure 19 Colored Schlieren Photograph of Interaction for 13° Shock

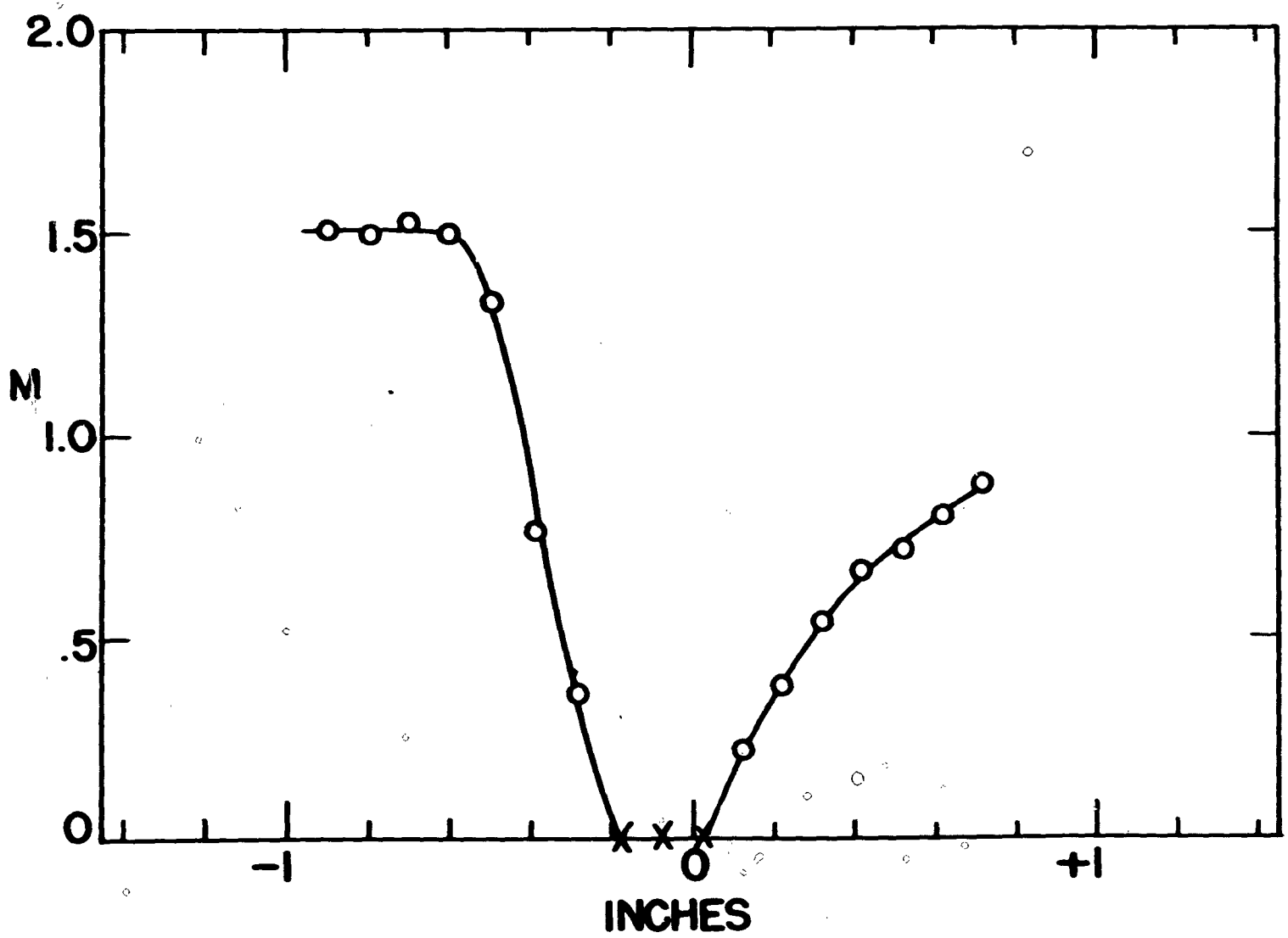

Figure 20 Mach Number Distribution .014 Inches from Wall for 10° Shock

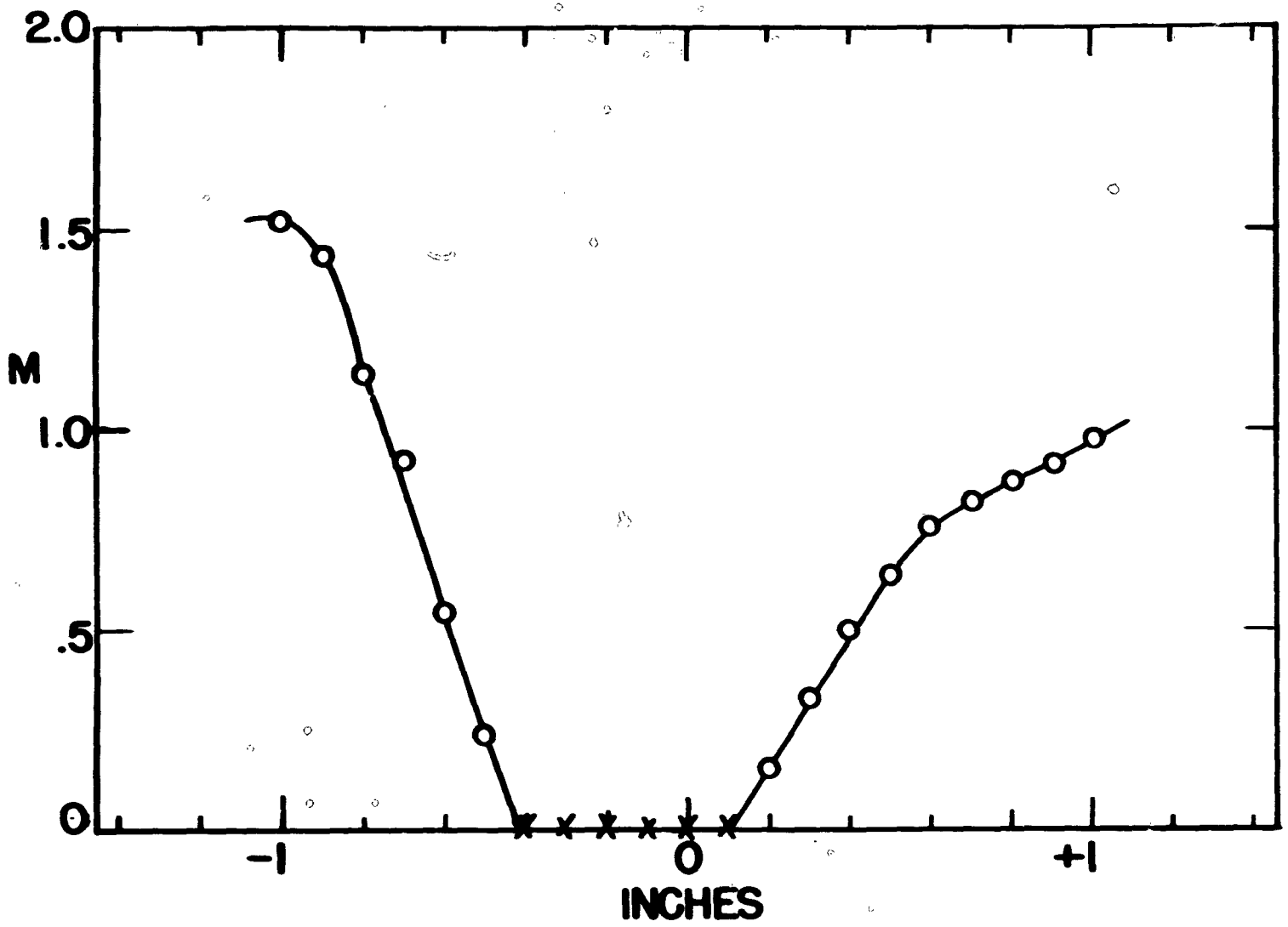

Figure 21 Mach Number Distribution .014 Inches from Wall for 12° Shock

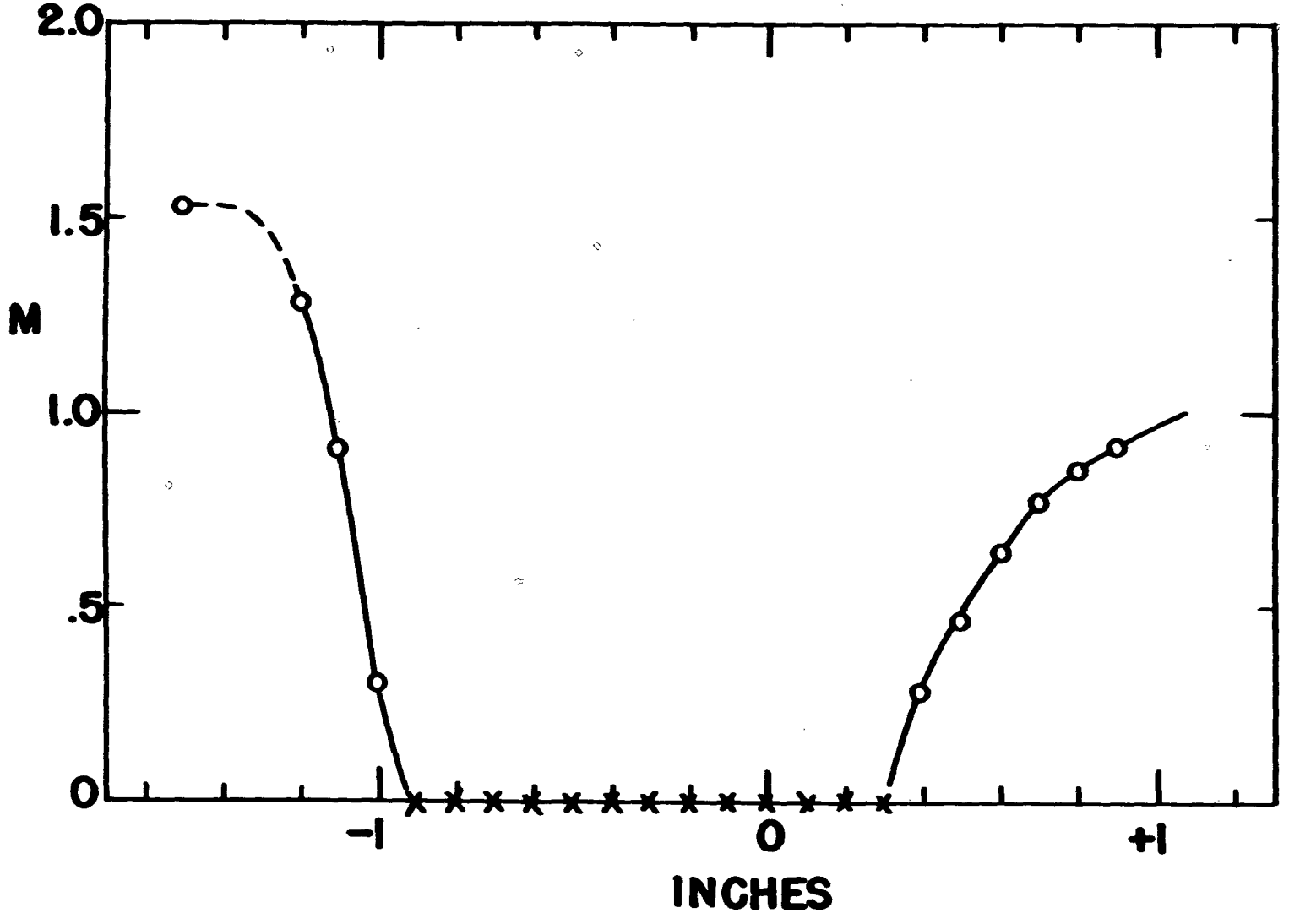

Figure 22 Mach Number Distribution .014 Inches from Wall for 14° Shock

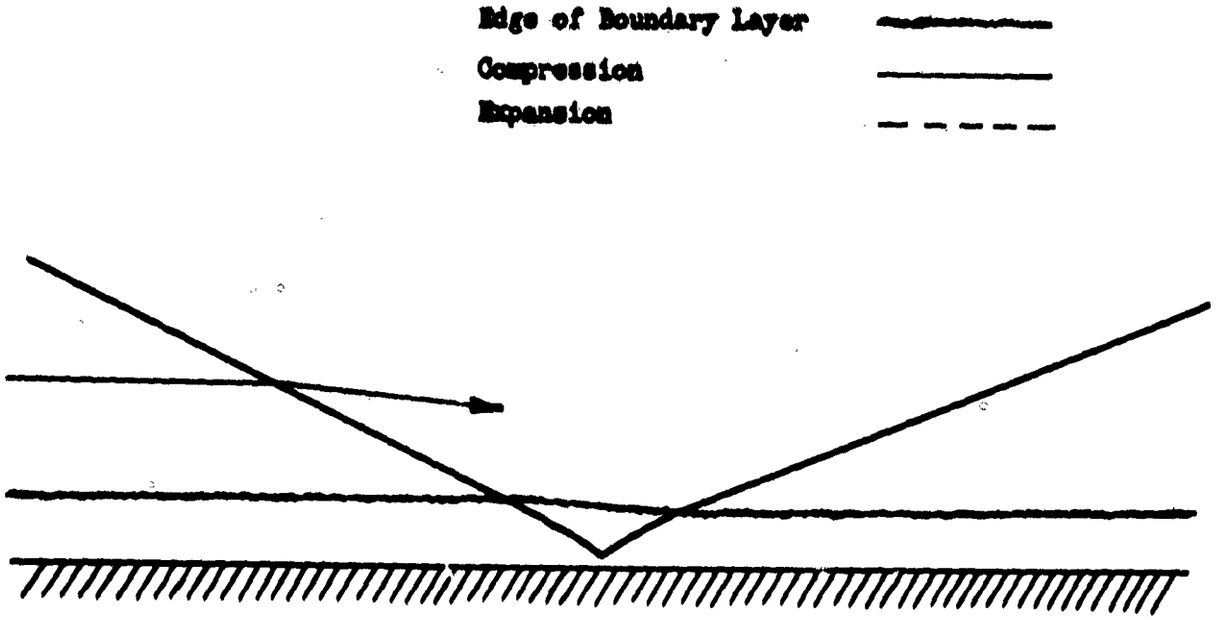

Weak Incident Shock $\theta \ll 7^{\circ}$

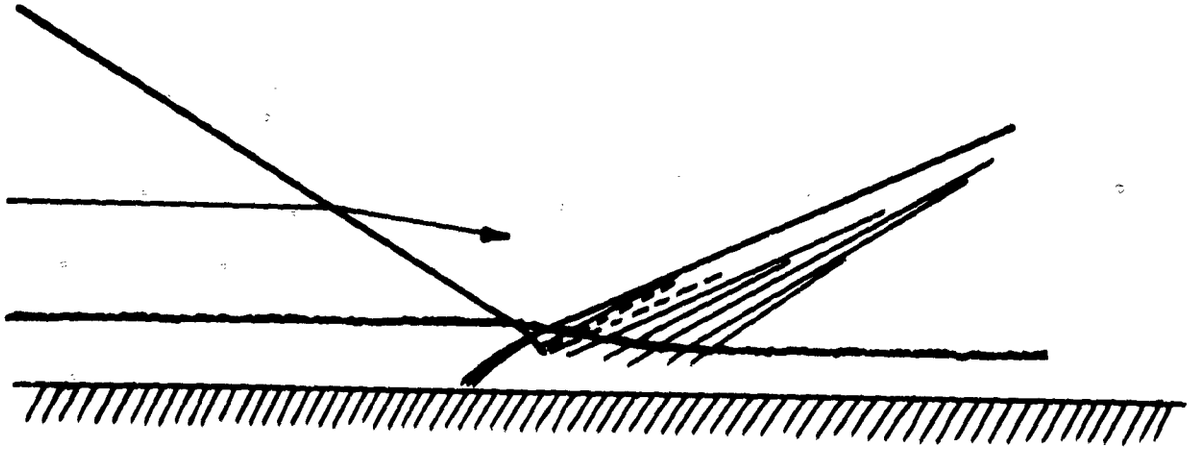

Medium Strength Shock $\theta \sim 9^{\circ}$

Figure 23 Sketch of Interaction Region with Varying Strength Shocks

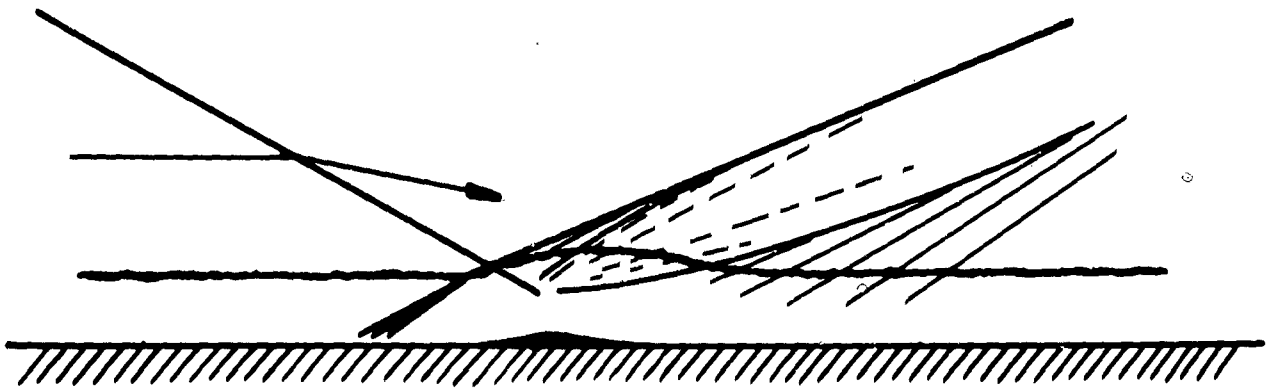

Medium Strength Shock $\theta \sim 11^{\circ}$

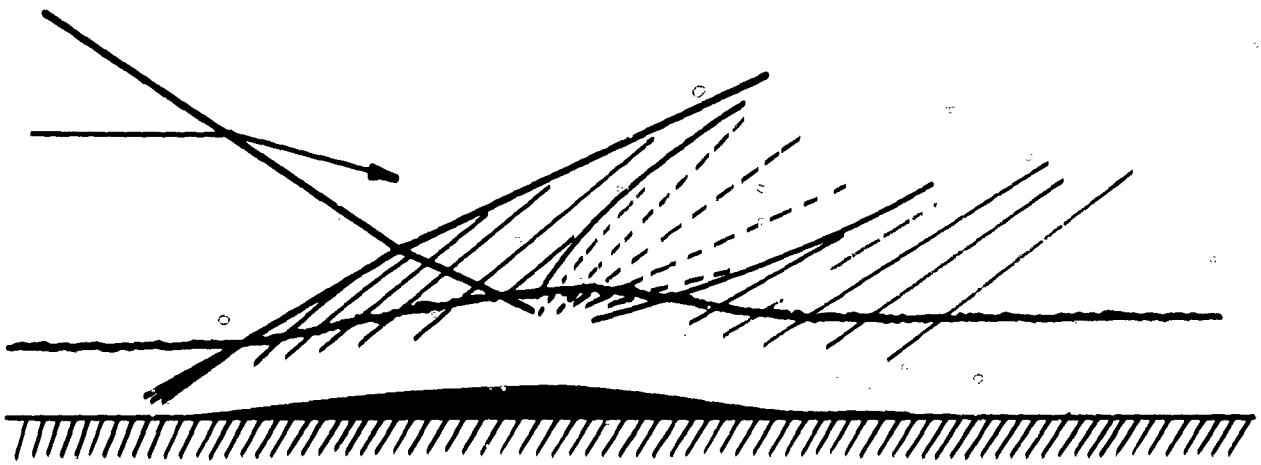

Strong Incident Shock $\theta \geq 13^{\circ}$

Figure 23 Concluded

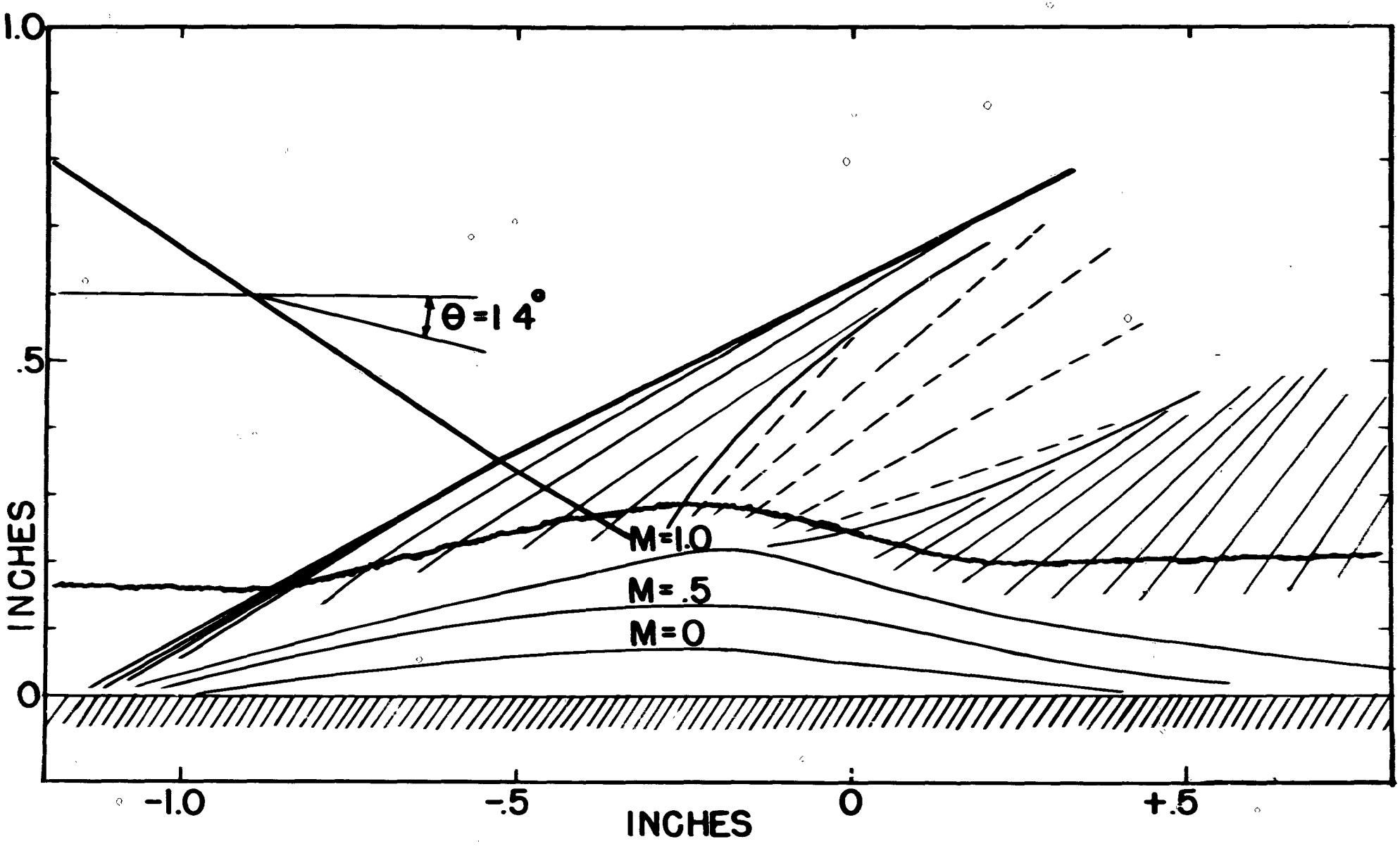

Figure 24 Sketch of Interaction for 14° Shock Showing the Contours of Constant Mach Number in the Subsonic Region

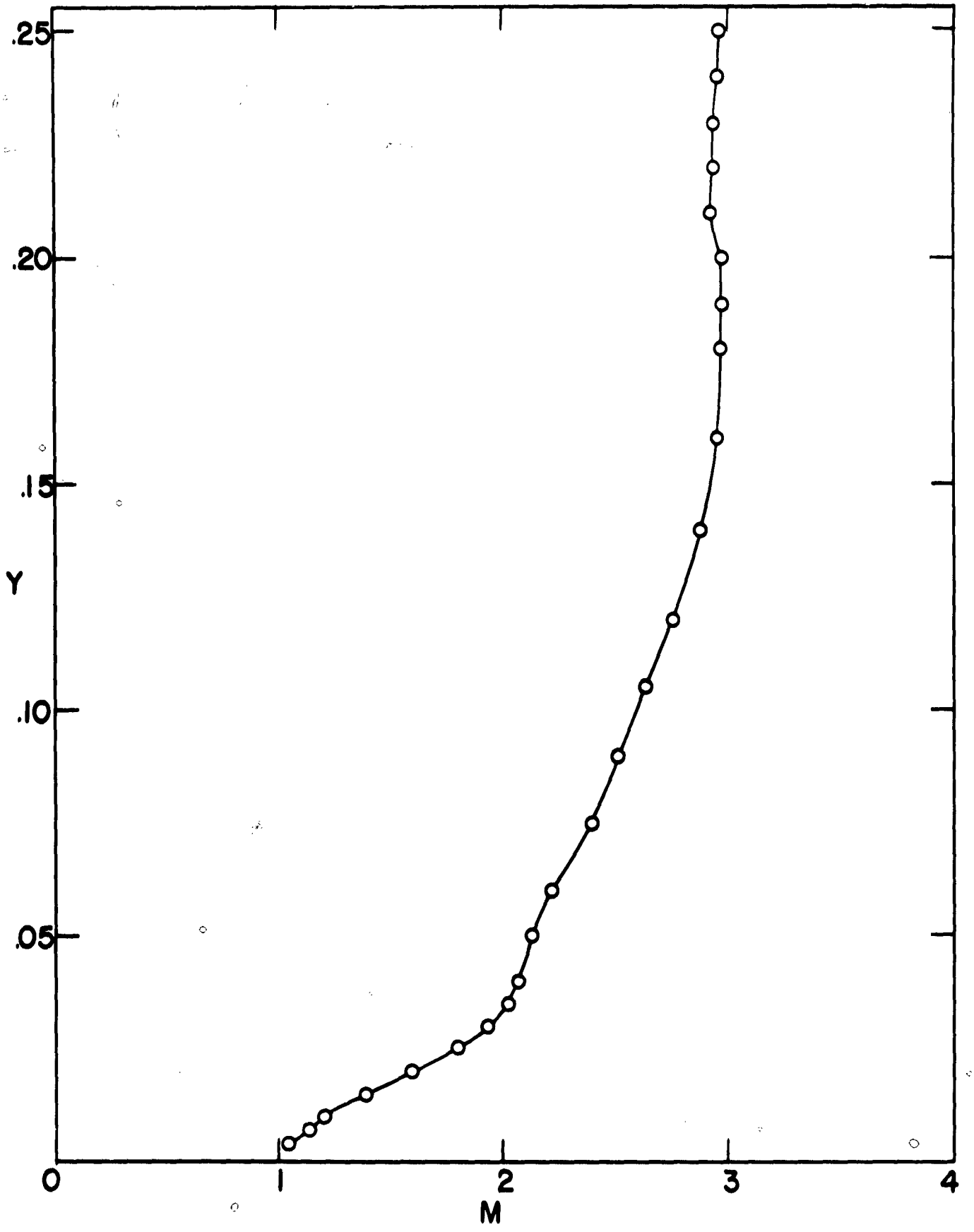

Figure 25 Mach Number Profile Through the Boundary Layer at Various Stations x = -.7

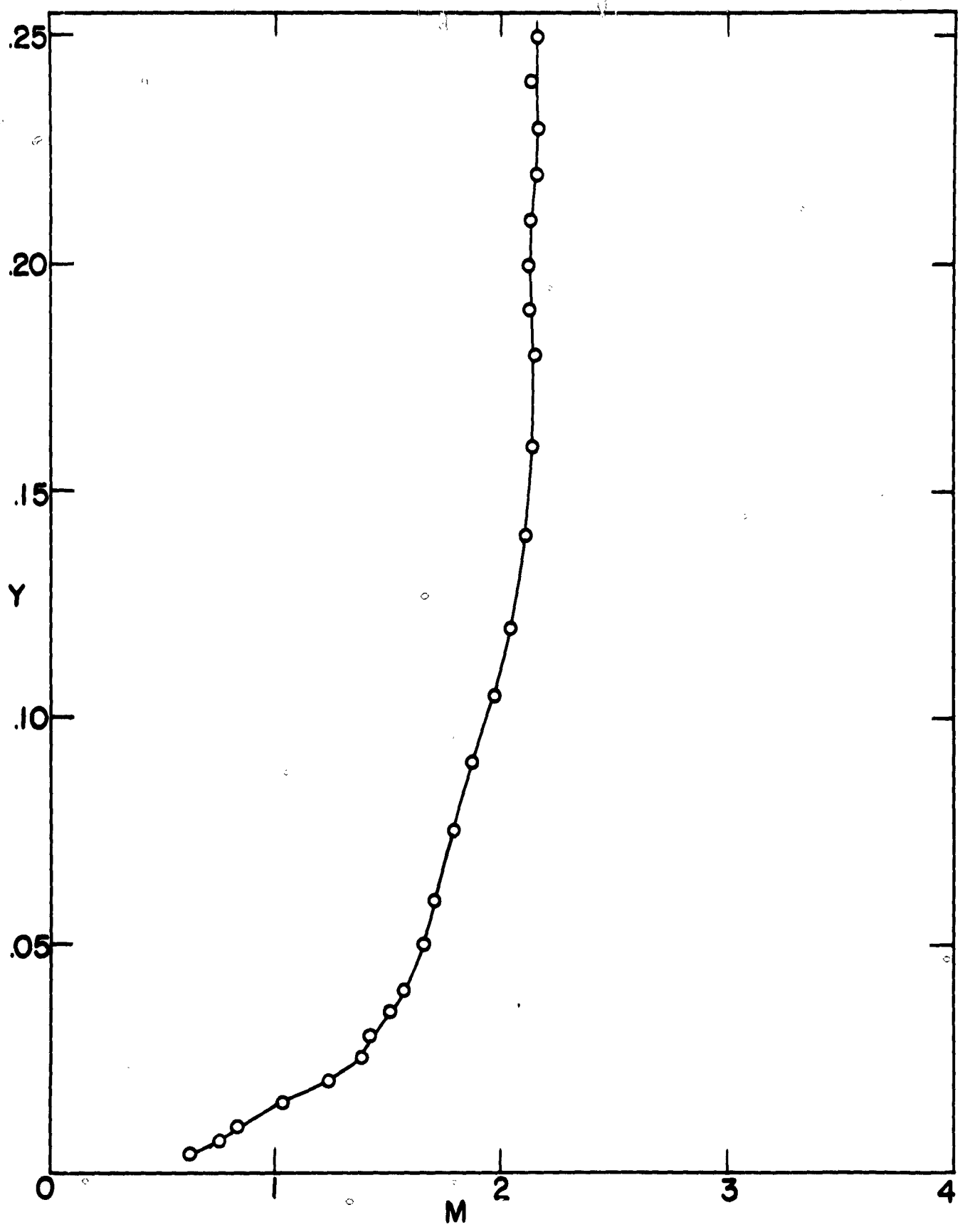

Figure 25 Continued $x = -.4$

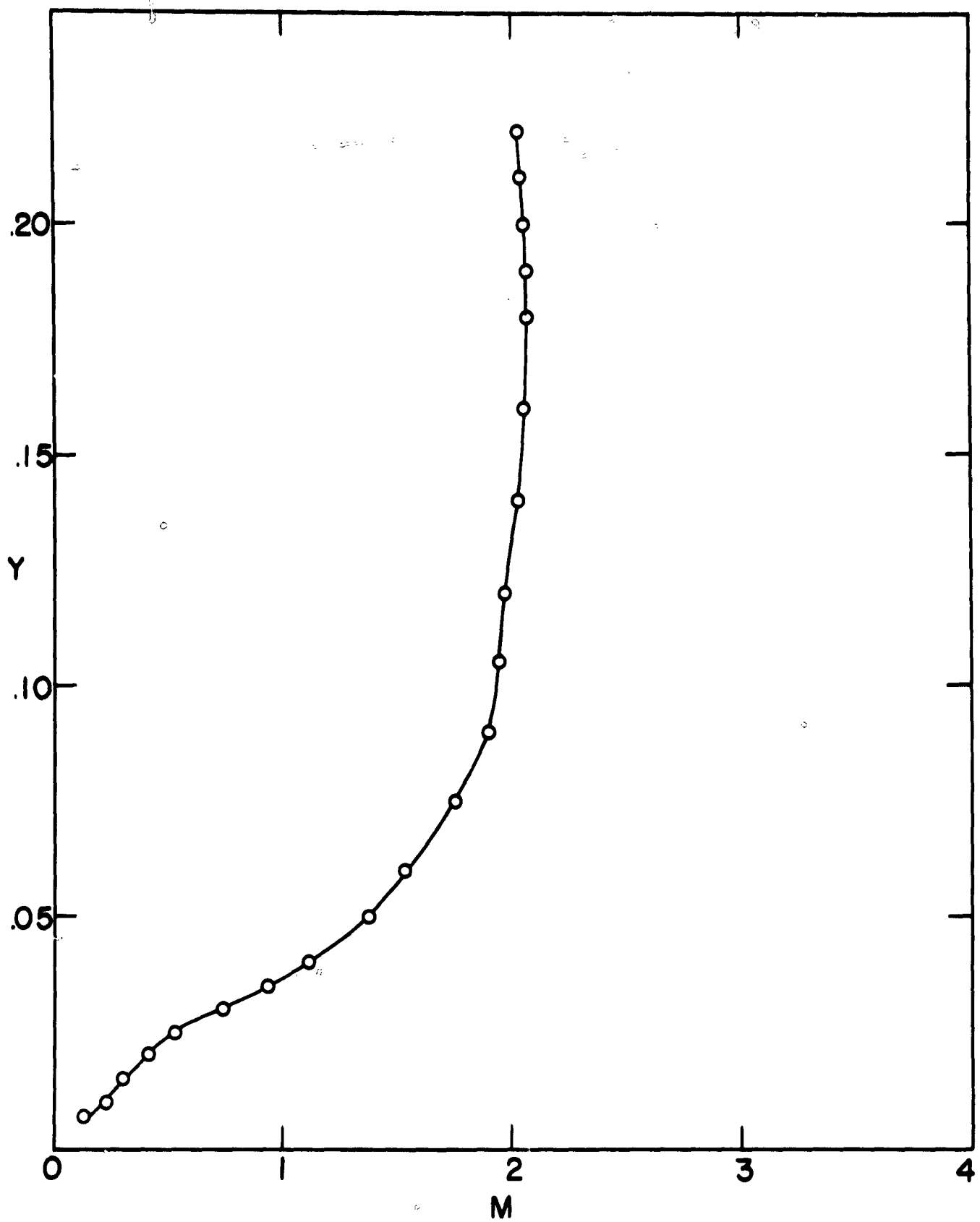

Figure 25 Continued x = -.3

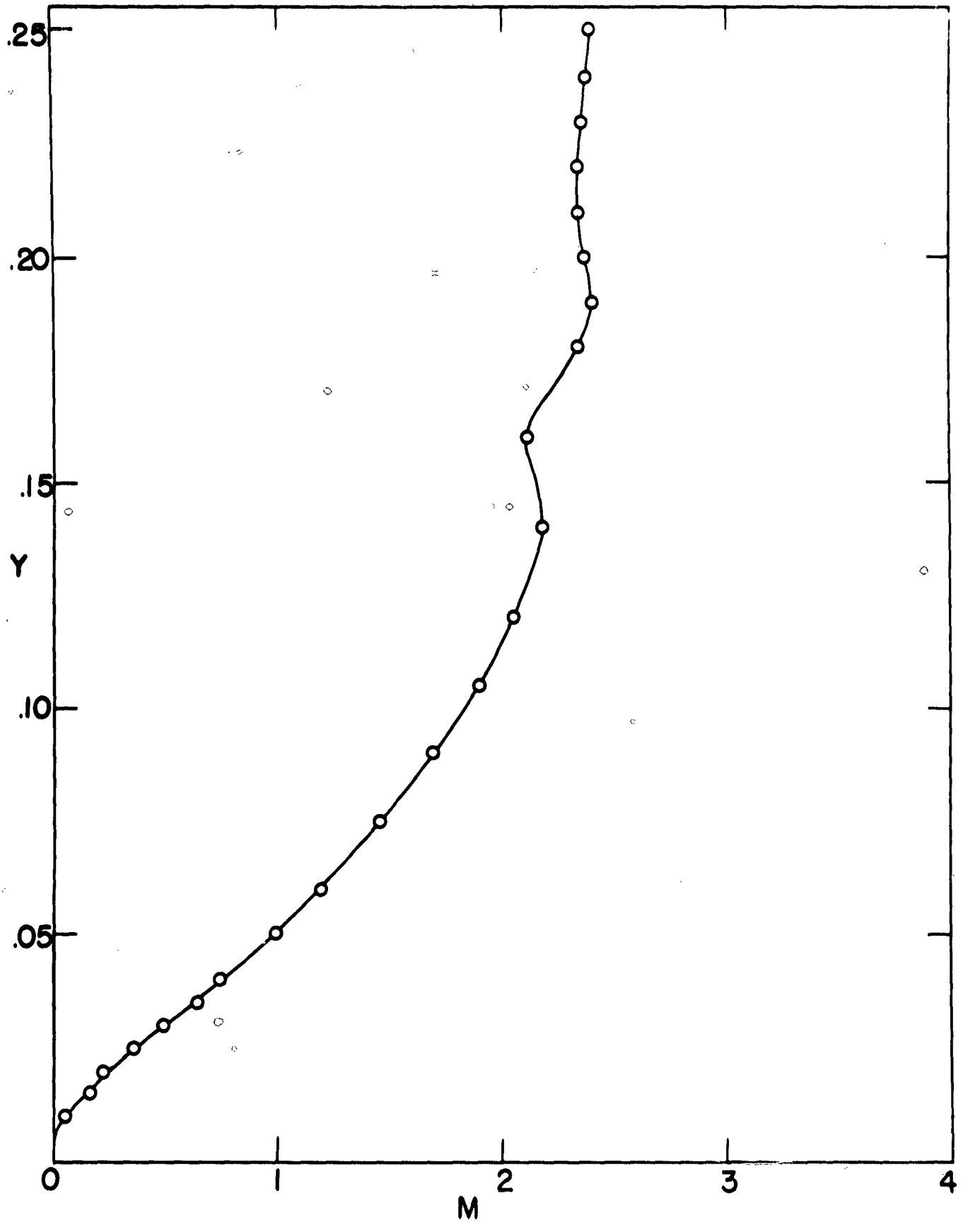

Figure 25 Continued

x = -.2

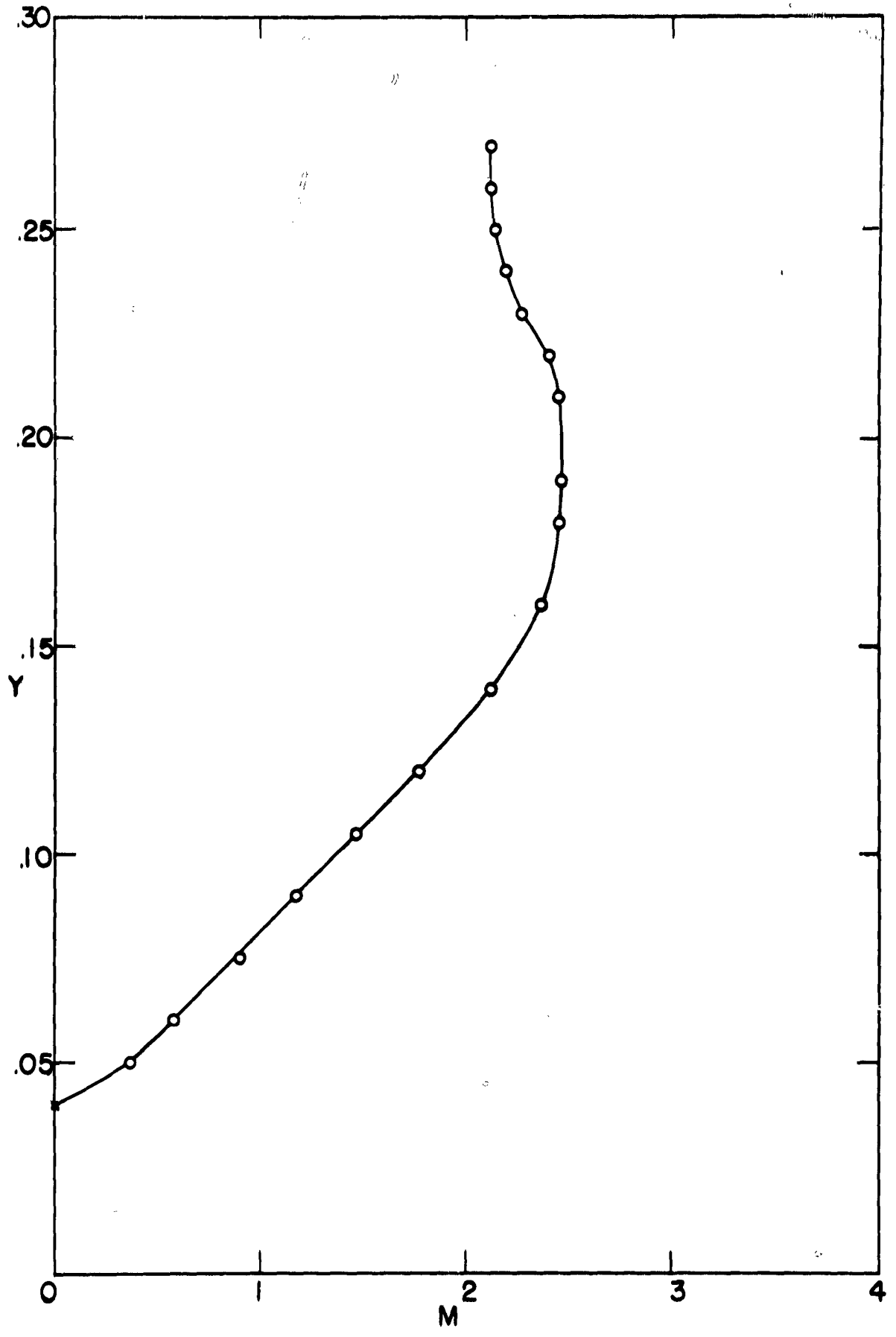

Figure 25 Continued

x = 0

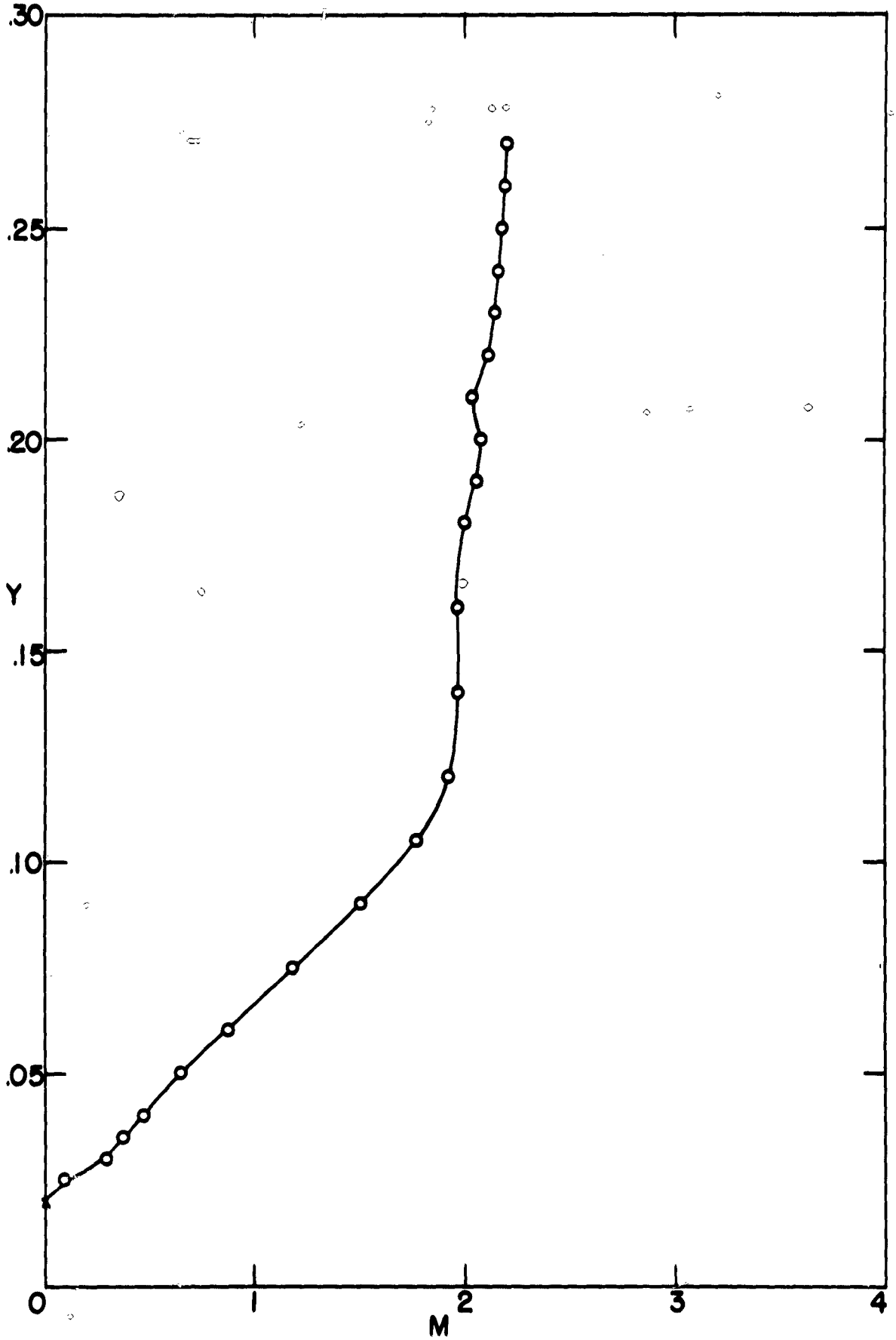

Figure 25 Continued $x = +.2$

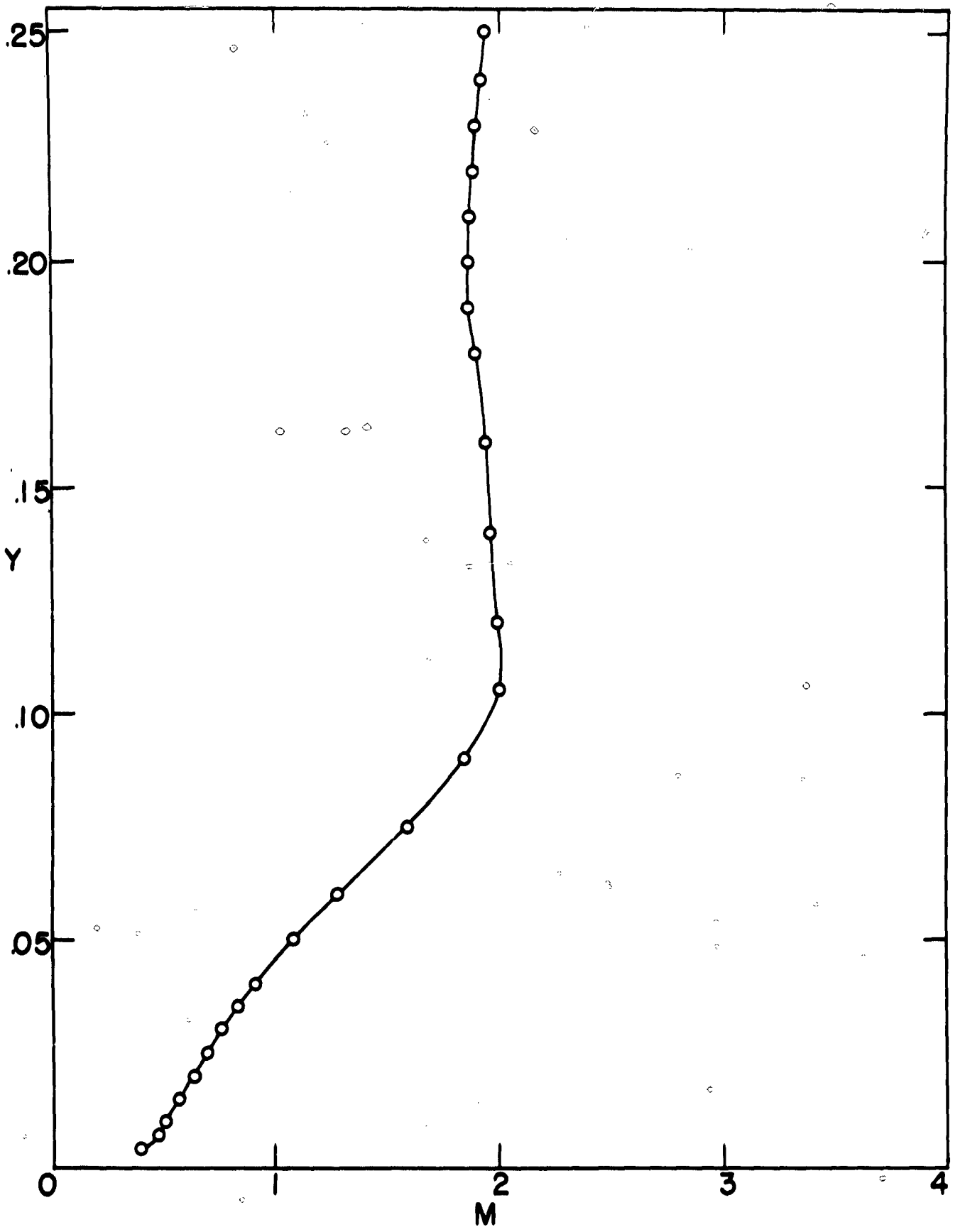

Figure 25 Continued

x = +.4

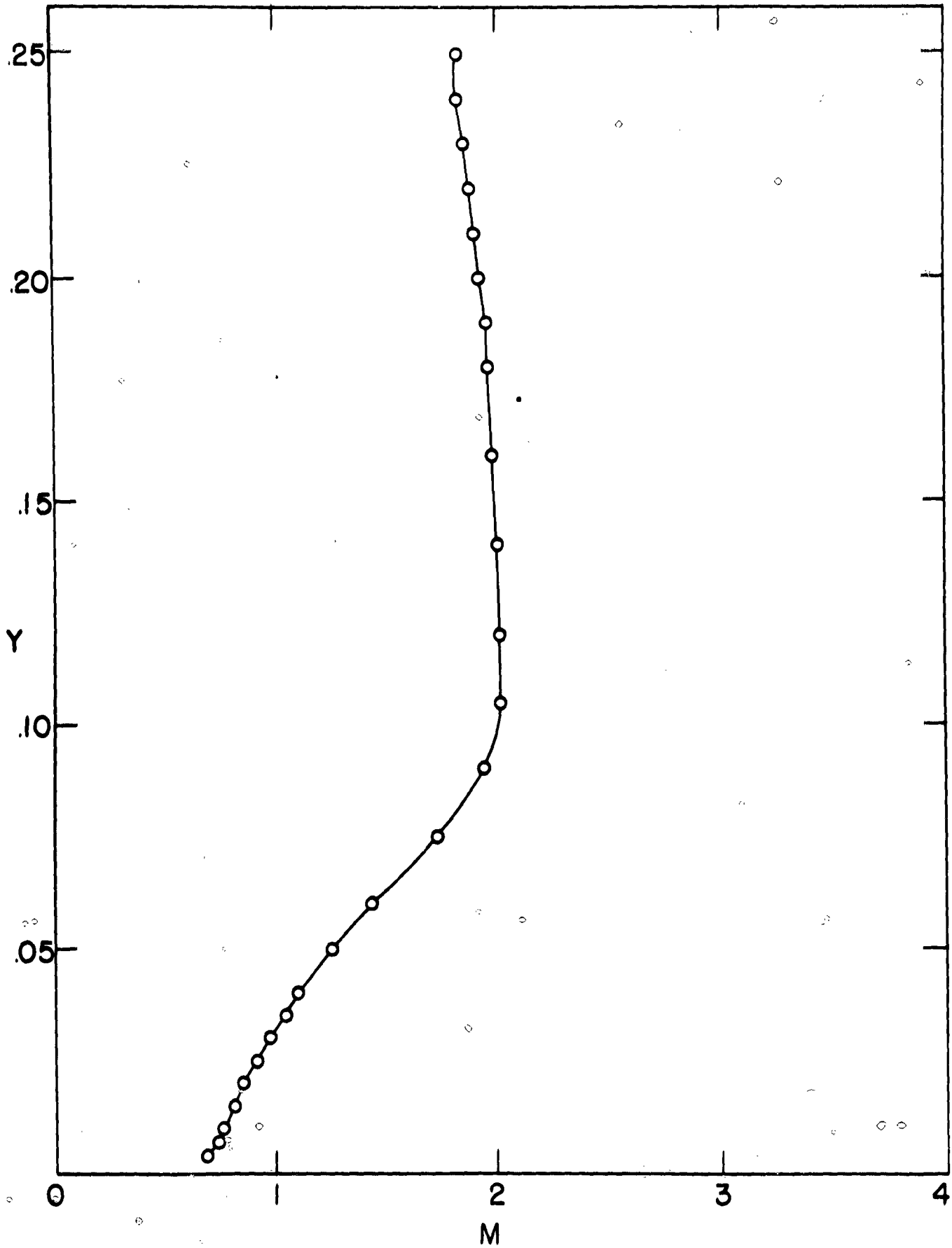

Figure 25 Continued x = 4.6

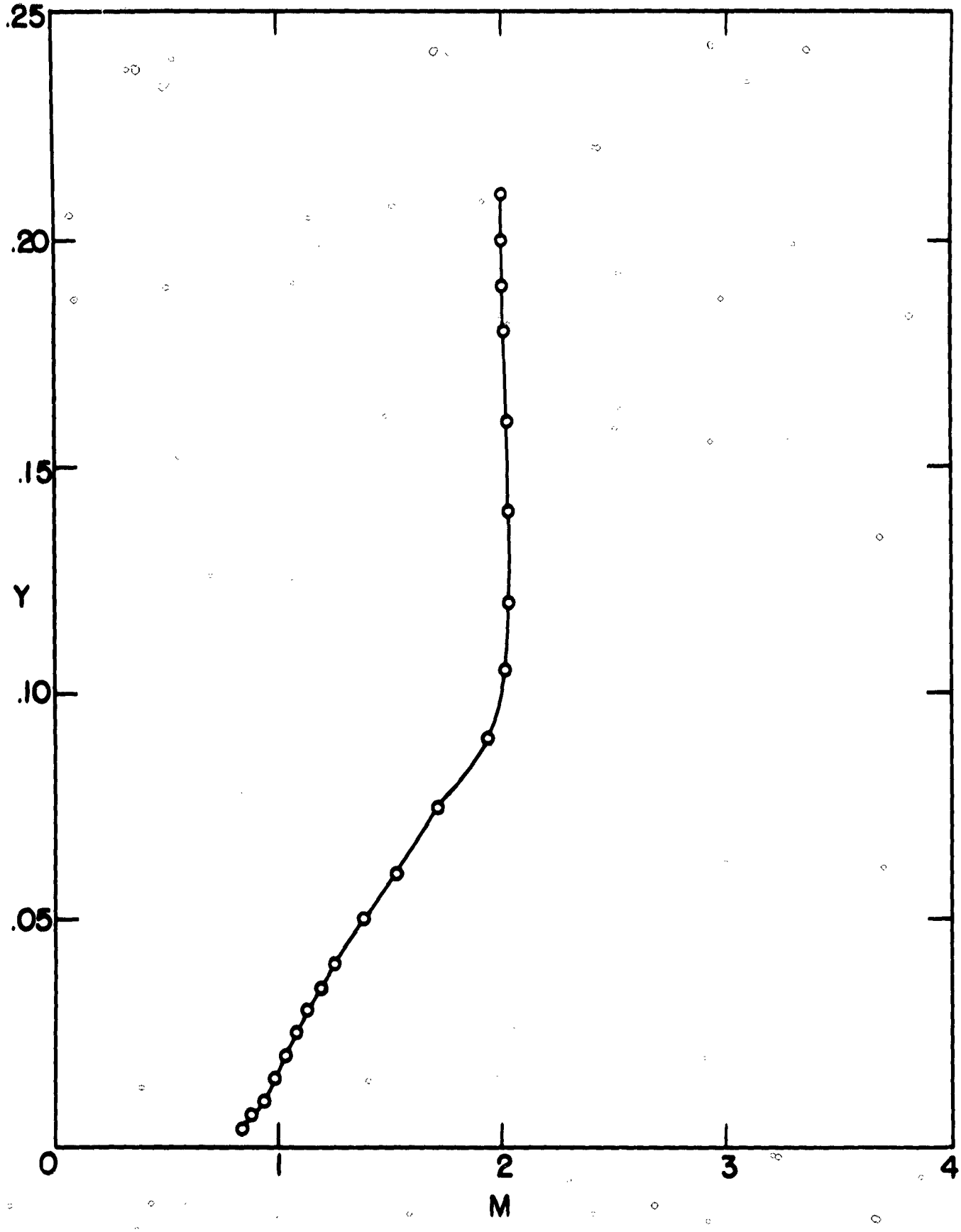

Figure 25 Continued $x = +.8$

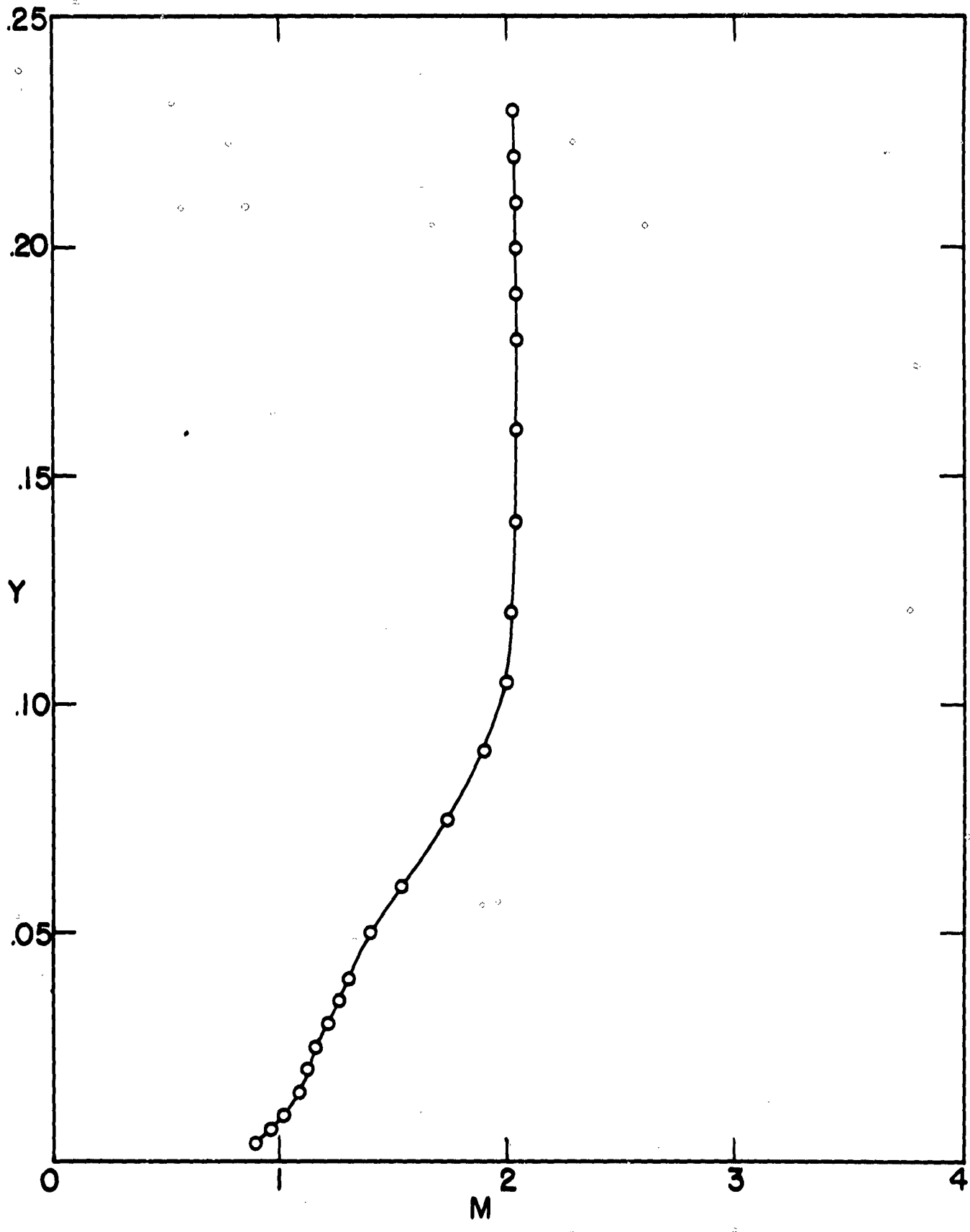

Figure 25 Continued x = +1.0

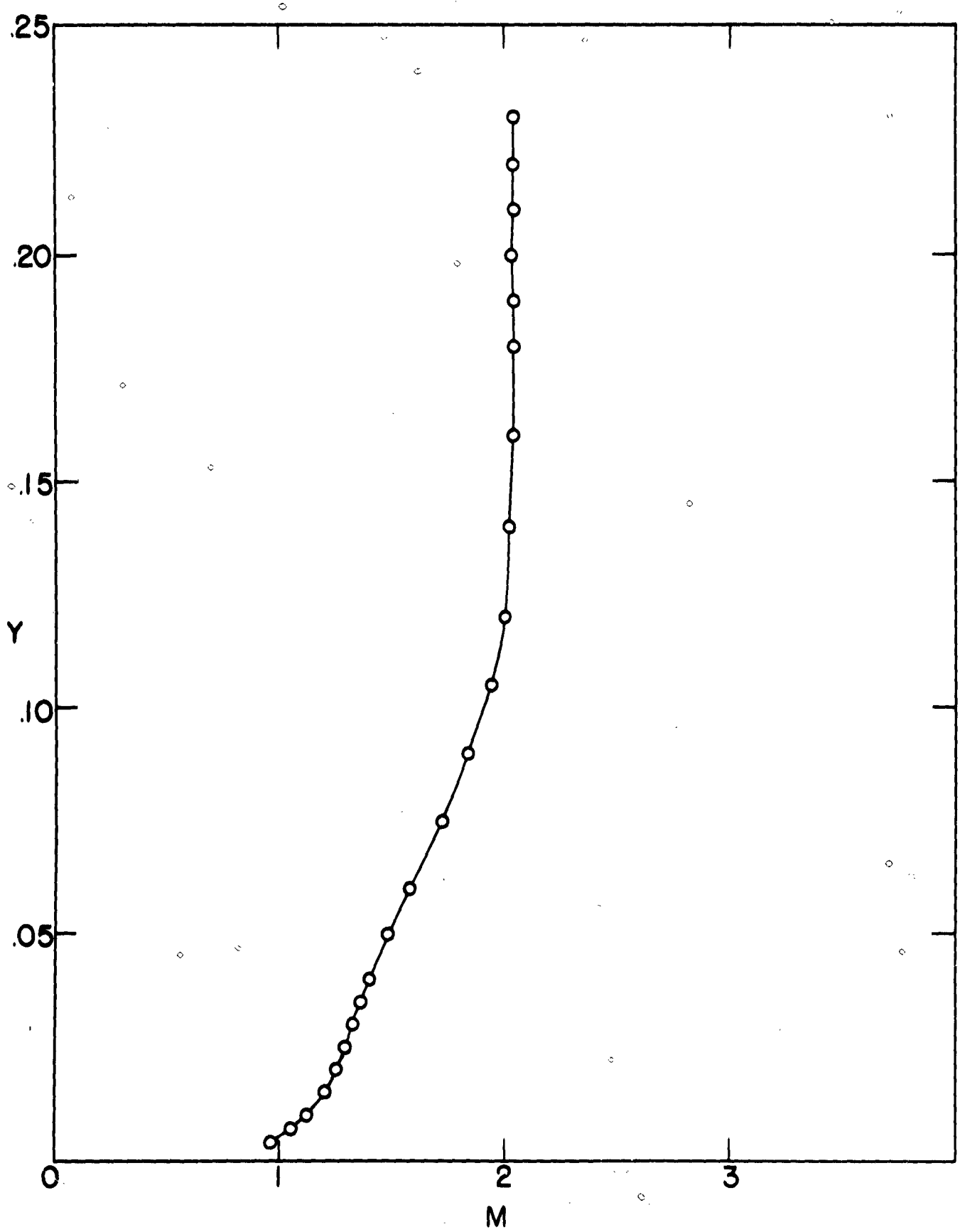

Figure 25 Continued x = +1.3

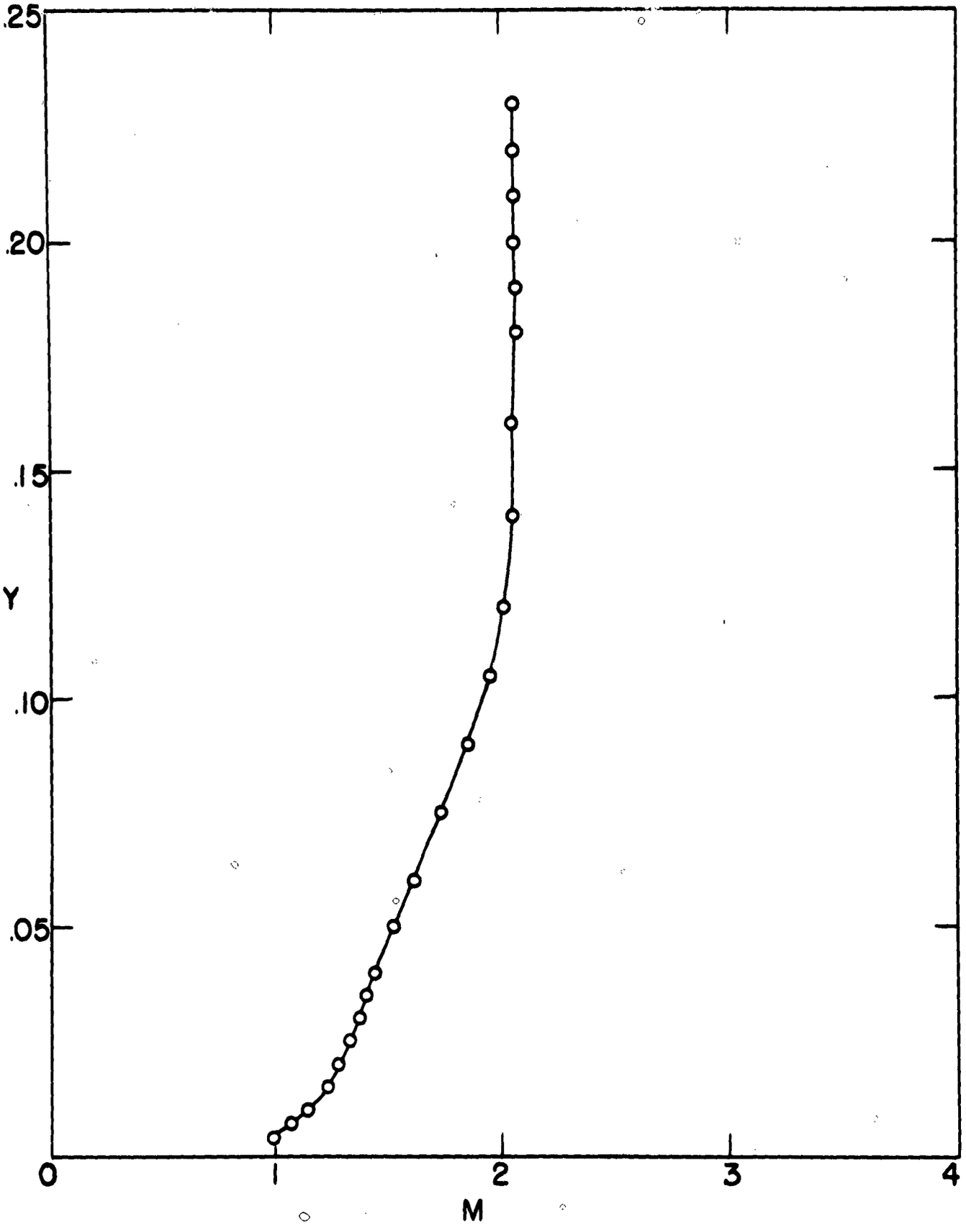

Figure 25 Concluded

x = +1.6

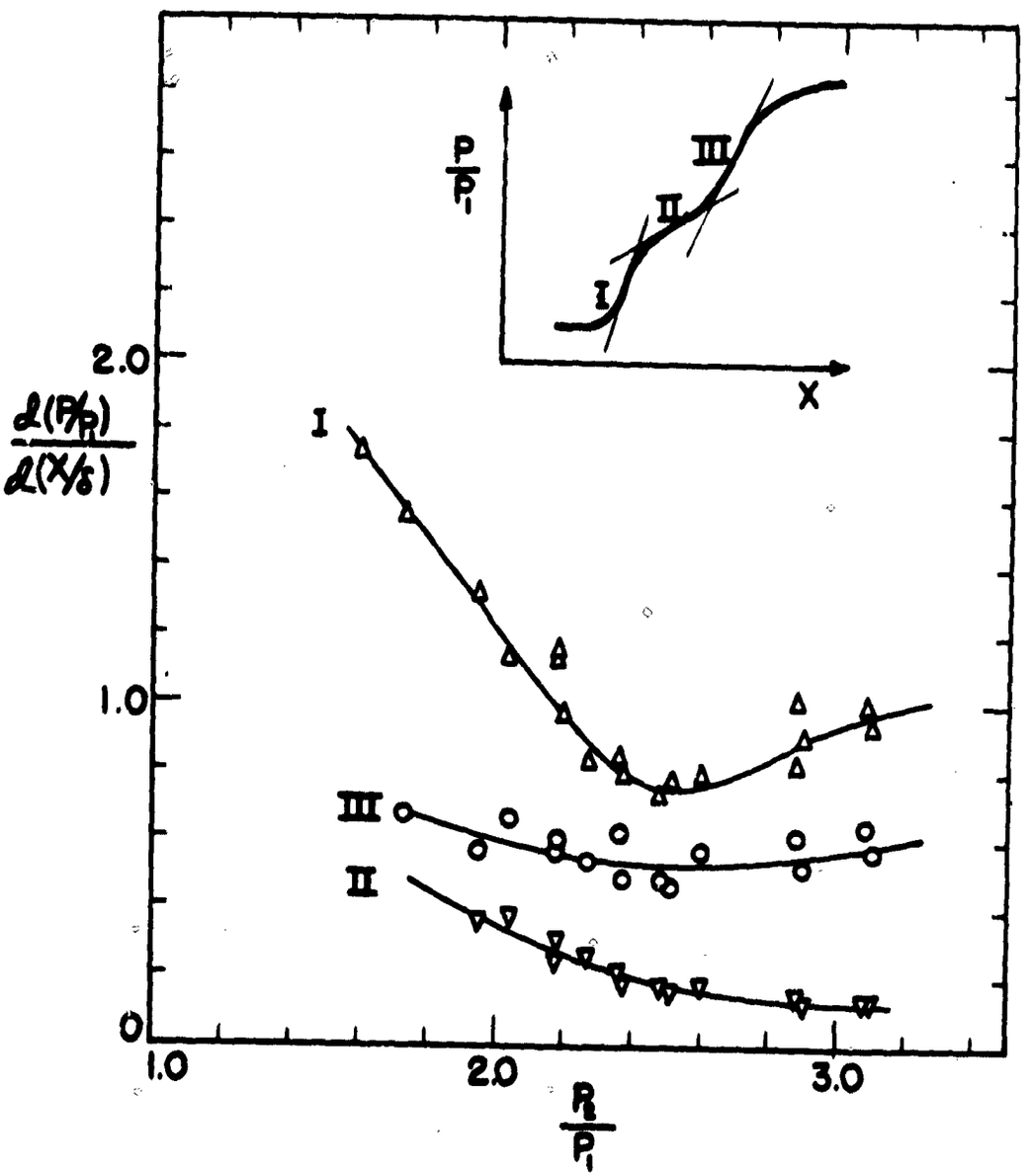

Figure 26 Synopsis of Wall Static Pressure Gradients for Varying Incident Shock Pressure Ratios

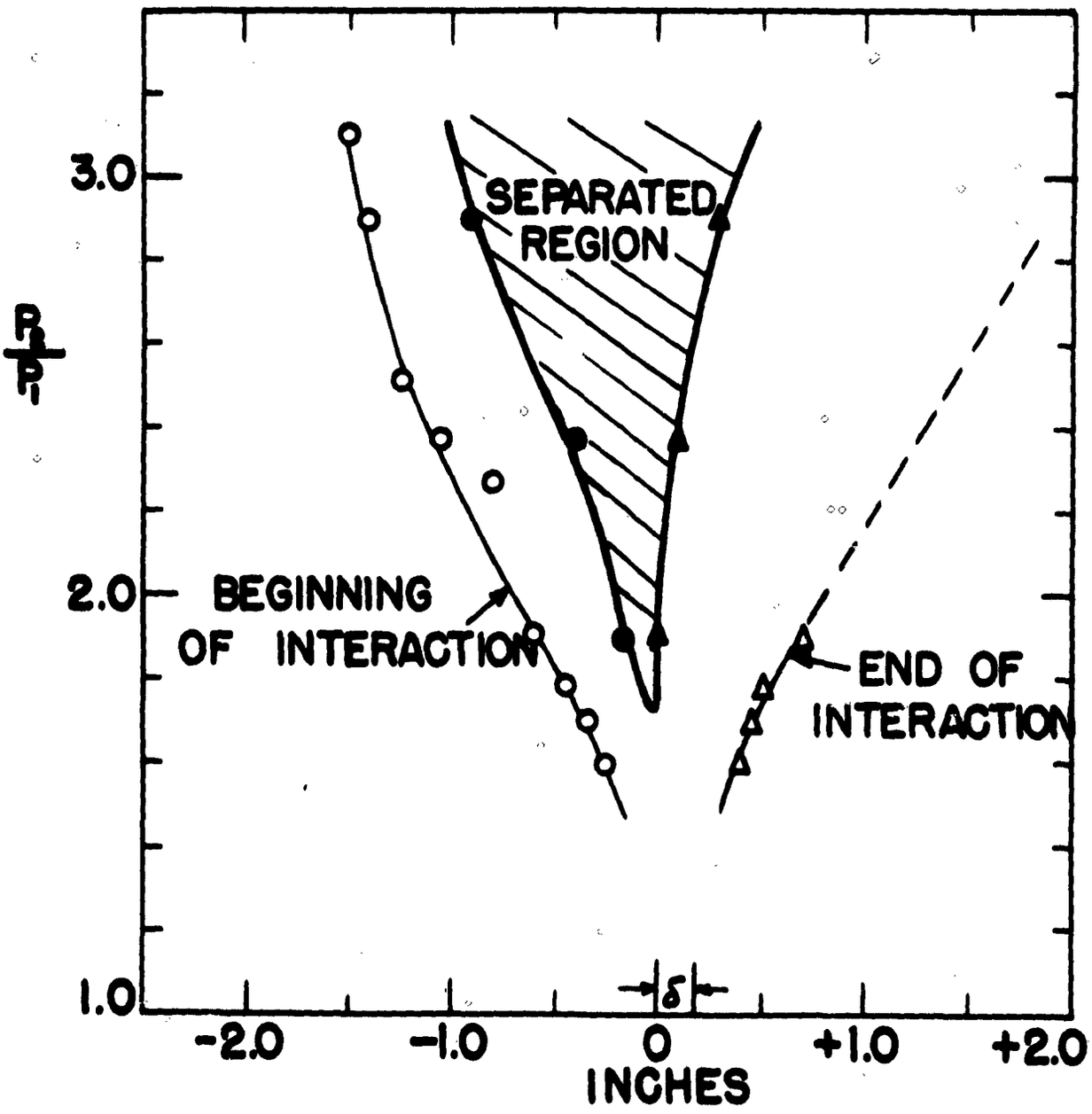

Figure 27 Extent of Interaction and Separated Regions for Varying Incident Shock Pressure Ratios